AMERICAN SOCIETY FOR MICROBIOLOGY | Journal of Virology®

VIRUS-CELL INTERACTIONS

The Reovirus μ2 C-Terminal Loop Inversely Regulates NTPase and Transcription Functions versus Binding to Factory-Forming μNS and Promotes Replication in Tumorigenic Cells

Wan Kong (Wynton) Yip,[a] Francisca Cristi,[a] Georgi Trifonov,[a] Nashae Narayan,[a] Mark Kubanski,[a] Maya Shmulevitz[a]

[a]Department of Medical Microbiology and Immunology, Li Ka Shing Institute of Virology, University of Alberta, Edmonton, Alberta, Canada

ABSTRACT The wild-type reovirus serotype 3 Dearing PL strain (T3wt) is being heavily evaluated as an oncolytic and immunotherapeutic treatment for cancers. Mutations that promote reovirus entry into tumor cells were previously reported to enhance oncolysis; here, we aimed to discover mutations that enhance the postentry steps of reovirus infection in tumor cells. Using directed evolution, we found that reovirus variant T3v10^{M1} exhibited enhanced replication relative to that of T3wt on a panel of cancer cells. T3v10^{M1} contains an alanine-to-valine substitution (A612V) in the core-associated μ2, which was previously found to have nucleoside-triphosphatase (NTPase) activities in virions and to facilitate virus factory formation by association with μNS. Paradoxically, the A612V mutation in μ2 from T3v10^{M1} was discovered to impair NTPase activities and RNA synthesis, leading to a 5-fold higher probability of abortive infection for T3v10^{M1} relative to that with T3wt. The A612V mutation resides in a previously uncharacterized C-terminal region that juxtaposes the template entry site of the polymerase μ2; our findings thus support an important role for this domain during virus transcription. Despite crippled onset of infection, T3v10^{M1} exhibited greater accumulation of viral proteins and progeny during replication, leading to increased overall virus burst size. Both far-Western blotting and coimmunoprecipitation (Co-IP) approaches corroborated that the A612V mutation in μ2 increased association with the nonstructural virus protein μNS and enhances burst size. Together, the data show that mutations in the C-terminal loop domain of μ2 inversely regulate NTPase and RNA synthesis versus interactions with μNS, but with a net gain of replication in tumorigenic cells.

IMPORTANCE Reovirus is a model system for understanding virus replication and also a clinically relevant virus for cancer therapy. We identified the first mutation that increases reovirus infection in tumorigenic cells by enhancing postentry stages of reovirus replication. The mutation is in a previously uncharacterized C-terminal region of the M1-derived μ2 protein, which we demonstrated affects multiple functions of μ2, namely, NTPase, RNA synthesis, inhibition of antiviral immune response, and association with the virus replication factory-forming μNS protein. These findings promote a mechanistic understanding of viral protein functions. In the future, the benefits of μ2 mutations may be useful for enhancing reovirus potency in tumors.

KEYWORDS NTPase, RNA transcription, reovirus, virus factory, mu2, oncolytic viruses

Mammalian orthoreovirus (MRV) is a nonenveloped, icosahedral, and nonpathogenic virus in the *Reoviridae* family (1, 2). Its 10 genomic double-stranded RNA (dsRNA) segments are classified by size as follows: 4 small (S1 to S4), 3 medium (M1 to M3), and 3 large (L1 to L3). These genes encode 8 structural proteins composing the outer capsid and inner core of the virion and 4 nonstructural proteins that are *de novo*

Citation Yip WKW, Cristi F, Trifonov G, Narayan N, Kubanski M, Shmulevitz M. 2021. The reovirus μ2 C-terminal loop inversely regulates NTPase and transcription functions versus binding to factory-forming μNS and promotes replication in tumorigenic cells. J Virol 95:e02006-20. https://doi.org/10.1128/JVI.02006-20.

Editor Rebecca Ellis. Dutch, University of Kentucky College of Medicine

Address correspondence to Maya Shmulevitz, shmulevi@ualberta.ca.

Received 9 October 2020
Accepted 20 February 2021
Accepted manuscript posted online 3 March 2021
Published 26 April 2021

synthesized in infected cells to aid viral replication (3). Reovirus infects a wide range of mammalian hosts and is classified into 4 serotypes, namely type 1 Lang (T1L), type 2 Jones (T2J), type 3 Abney (T3A) and Dearing (T3D), and type 4 Ndelle (T4N) (4, 5). Of clinical relevance, the wild-type (wt) T3D strain from the Patrick Lee laboratory (T3D-PL, here referred to as T3wt) exploits and selectively replicates in cancer cells, which often have impaired antiviral responses and other advantages conferred to reovirus over nontransformed cells (6, 7). T3wt is in clinical trials as a therapy for numerous cancers (8), in conjunction with other traditional therapies such as immunotherapies, chemotherapeutics, and radiation (9–11). In 2015, T3wt received orphan drug designation from FDA for malignant glioma, ovarian cancer, and pancreatic cancer (12).

During natural infection, reovirus evolved to infect the enteric and respiratory tracts, and may therefore not yet be optimized to replicate in cancer cells. Based on this rationale, a few past studies have aimed to improve the virus potency in tumors. A number of reovirus variants have been described to possess enhanced oncolytic potency and increased specificity toward cancer cells, suggesting that reovirus can be further adapted to infect cancer cells (13–16). All variants described thus far have an advantage at the entry steps of infection, such as host cell binding or virus uncoating, and are associated with mutations that exclusively alter structural proteins on the outer capsid of the virus. For example, mutations in the reovirus cell attachment protein σ1 that impart an optimal level of σ1 per virion were found to increase virus uncoating, enhance infectivity in cancer cells, and promote oncolytic activities *in vivo* (17, 18). It remained unknown whether mutations in reovirus could also promote post-entry steps of virus replication in tumor cells; such mutations may serve utility in further enhancing reovirus oncolytic efficiency and also provide a better understanding of reovirus replication and protein functions.

In the current study, we discovered a reovirus variant with enhanced replication in tumor cells (T3v10^{M1}) that contains a mutation in the M1 gene-encoded μ2 protein. Since μ2 is not involved in virus entry, it became of interest for further mechanistic exploration. The μ2 protein is a multifunctional viral protein with two roles. First, as a structural component residing at the vertices of reovirus particles, μ2 associates with the polymerase λ3 and fulfills polymerase cofactor functions (19). Specifically, μ2 possesses nucleoside-triphosphatase (NTPase) activities (20–22), has putative NTP-binding motifs (22, 23), binds single-stranded RNA (ssRNA) and dsRNA nonspecifically (24), and affects reovirus transcription (25). Newly synthesized μ2 also serves a second function, that of supporting the formation of localized sites of reovirus replication called "factories" (26–30). Specifically, μ2 bridges cellular microtubules (MT) to μNS, a viral nonstructural protein responsible for recruiting viral proteins to factories for assembly (29, 31). Recent studies demonstrated that μ2 is essential during reovirus replication in an MT-dependent manner, and identified μ2 regions that are important for MT, μNS, and self-association (32–37). It is interesting for the current study that the mutation in μ2 of T3v10^{M1} resides in a C-terminal loop that has not previously been implicated in either of the μ2 functions. The enhanced replication of T3v10^{M1} in cancer cells prompted us to examine the role(s) of the μ2 C-terminal loop.

Paradoxically, the results of this study demonstrate that the μ2 C-terminal loop mutation in T3v10^{M1} imparted both replication-enhancing and -restricting effects on reovirus replication, with an overall net benefit of increased infectivity toward tumor cells. Specifically, the A612V mutation in μ2 reduced the NTPase and core transcription activities, leading to a reduced probability that incoming cores establish productive infection. Reciprocally, the mutation promoted interactions of μ2 with μNS both in cell and *in vitro*, enhancing T3v10^{M1} burst size by 3-fold in a single replication cycle. Overall, these studies are the first to report important roles for the μ2 C-terminal loop for both μ2 functions. The opposing effects of mutating the C-terminal loop on the two functions of μ2 reflect the challenge viruses must face when optimizing multifunctional proteins for distinct activities.

RESULTS

A mutation in reovirus M1-encoded μ2 promotes replication on cancer cells. As described in the introduction, we and other laboratories previously found it possible to improve the oncolytic potency of reovirus by adapting the virus toward tumorigenic cells. Since the mutations that promote reovirus oncolysis discovered so far exclusively promote early entry steps of reovirus infection (host cell binding and uncoating), we sought to identify novel mutations in reovirus that augment postentry replication steps so that ultimately such mutations could be combined additively to previously described adaptations. A directed evolution approach was used; specifically, mutant reoviruses that produced the largest virus plaques on a monolayer of L929 tumorigenic mouse fibroblasts were picked and propagated (Fig. 1A). Plaque size was chosen as the positive selection criterion, as it reflects possible enhancements at any stage of reovirus infection, including binding and uncoating, replication, and/or spread among cells. To increase reovirus mutagenesis, large plaques were chosen from lysates of wild-type (T3wt) reovirus generated in the presence of 5-fluorouracil. A reovirus variant (T3v10) was identified and confirmed to produce larger plaques than those of T3wt on a variety of tumorigenic cells following 5 days of infection, including PanC human pancreatic cancer cells and T47D human breast cancer cells (Fig. 1B). Plaque size was also determined concurrently for previously described large-plaque variants T3v1 and T3v2, which have lower σ1 per virion levels and thereby promote virus uncoating. Importantly, T3wt and all three variants only produced small foci of reovirus antigen-positive infected cells on nontransformed NIH3T3 fibroblasts even at 7 days postinfection, indicating restricted replication and spread in nontransformed cells (i.e., retained specificity toward transformed cells). Finally, plaque size on a panel of mouse and human cells was quantified for multiple experiments and presented as box-and-whisker plots (Fig. 1C); the data indicate a significant increase of plaque size for T3v10 relative to T3wt in tumorigenic cells, similarly to T3v1 and T3v2 (previously described), but not in nontransformed NIH3T3 cells.

To identify the mutations in T3v10, the 10 genome segments of T3v10 were PCR amplified and sequenced with at least 3 overlapping sequence reads per nucleotide. Relative to T3wt, T3v10 had two mutations. First, there was an adenine to guanine mutation at position 946 of the S1 genome segment, which produced an asparagine to arginine mutation (N312R) in the S1-encoded σ1 cell attachment protein. S1 also contains an internal open reading frame that encodes a second protein, σ1s, but the mutation in T3v10 was outside the coding sequence of this protein. Second, T3v10 also contained a cytosine to thymine mutation at position 1848 of the M1 genome segment, which introduced an alanine to valine mutation (A612V) in the M1-encoded μ2 protein.

The next objective was to determine whether one or both mutations in T3v10 contributed to large plaque size. Since the reovirus genome is segmented and the mutations were in different genome segments, reassortment analysis was used to separate the mutations in S1 and M1. L929 cells were coinfected with T3wt and T3v10, and 10 progeny virus plaques were selected and sequenced. One reassortant with wild-type S1 and M1 sequences (RA1), two reassortants with mutation only in S1 (RA2 and RA3), and two reassortants with mutation only in M1 (RA4 and RA5) were then assessed for plaque size relative to that of T3wt and T3v10 (Fig. 1D). The rationale for using two reassortant plaque pick for every monoreassortant was to account for possible secondary mutations that arise during virus propagation. Plaque size analyses indicated that mutations in S1 and M1 can independently increase reovirus plaque size relative to T3wt, without a significant additive advantage relative to T3v10.

Of the two mutations in T3v10, the μ2 mutation seemed most interesting for several reasons. First, σ1 is the cell attachment protein and has been linked primarily to cell attachment and entry (38), and although some evidence also suggests a correlation between S1 sequence and rate of cell death (39–41), it was less likely that σ1 mutations could promote the postentry steps of virus replication. Conversely, the reovirus μ2 protein has not been associated with the steps of virus binding and entry, but

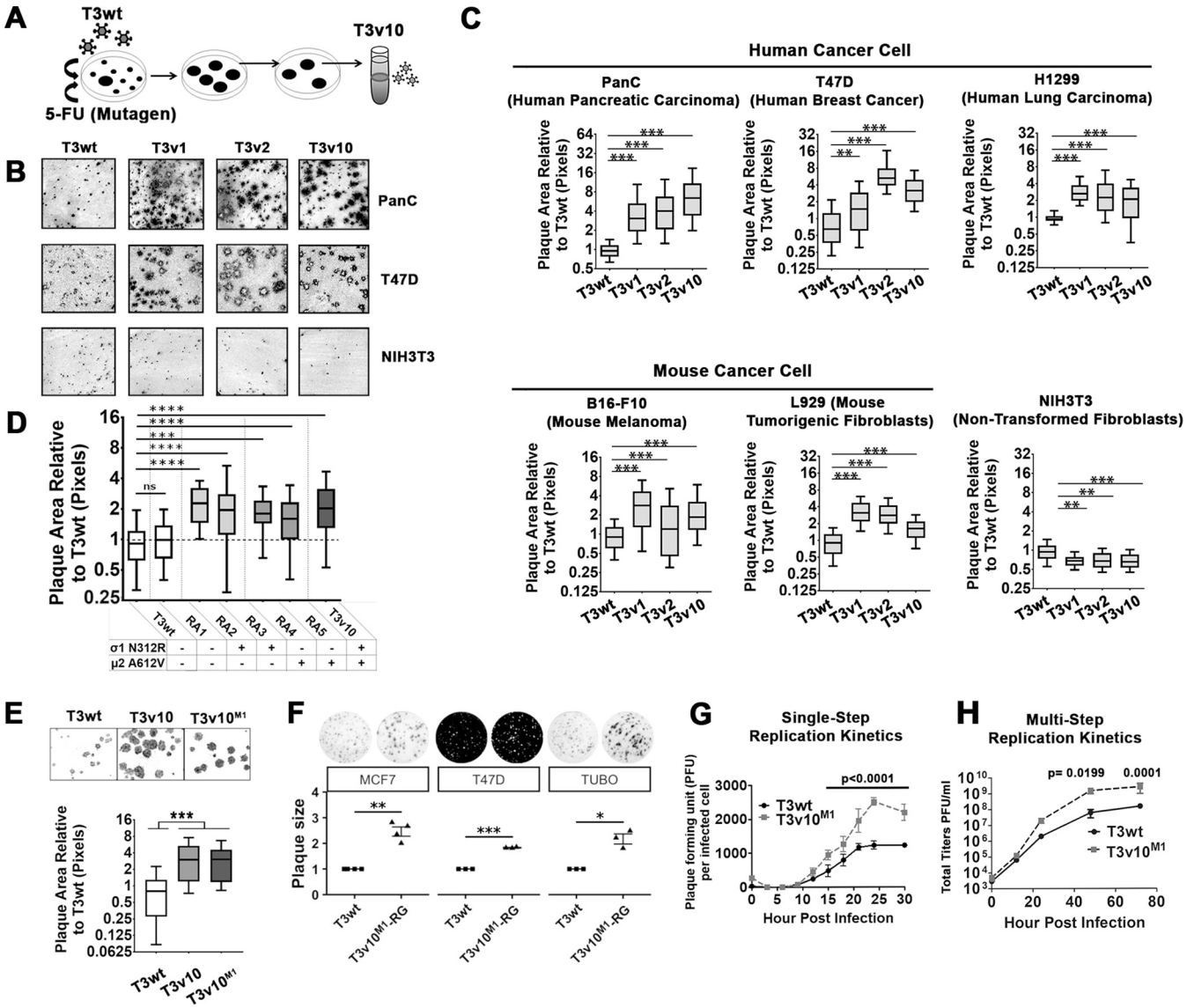

FIG 1 A mutation in reovirus M1-encoded $\mu 2$ promotes replication on cancer cells. (A) Schematic shows how wild-type reovirus T3wt was replicated in L929 tumorigenic mouse fibroblasts in the presence of 5-fluorouracil, generating variants (including T3v10) that produced larger plaques. (B) Plaque sizes of T3v10 were compared with those of previously characterized variants T3v1 and T3v2. All three variants selectively replicated in T47D (breast cancer) and PanC (pancreatic cancer) cells but had restricted replication in NIH3T3 (nontransformed mouse fibroblast). (C) Plaque sizes associated with each variant were compared in a panel of cell lines and represented by box-and-whisker plots ($n = 3$, mean ± standard deviation [SD]; one-way analysis of variance [ANOVA] with Dunnett's multiple-comparison test). (D) Mutations in $\sigma 1$ and $\mu 2$ found in T3v10 were segregated by coinfection of L929 cells with T3v10 and T3wt. Five reassortants (RA) containing single-gene mutations in $\sigma 1$ or $\mu 2$, as indicated, were subjected to plaque size analysis relative to parental viruses T3v10 and T3wt ($n = 2$, mean ± SD). (E) Plaque size of reassortant RA2 from (D), renamed T3v10^{M1}, was compared with those of T3wt, T3v10^{M1}, and parental viruses T3v10 in L929 cells ($n = 4$, mean ± SD; one-way ANOVA with Dunnett's multiple-comparison test). (F) Plaque size of T3wt and T3v10^{M1} created by reverse genetics (RG) was evaluated in two human breast cancer cell lines (MCF7 and T47D) and a murine one (TUBO) ($n = 4$ for MCF7, $n = 3$ for T47D and TUBO; mean ± SE, *t* test). (G) Single-cycle progeny production per infected cell was compared between T3wt and T3v10^{M1}. L929 cells were infected with an infectious dose to equivalently infect ~70% of cells (T3wt multiplicity of infection [MOI] = 2.7; T3v10^{M1} MOI = 19.5). At indicated hours postinfection (hpi), cell lysates were subjected to plaque assay. To determine PFU per infected cells, total titers were normalized to the percentage of infected cells empirically determined for each independent experiment by flow cytometric analysis with polyclonal antireovirus antibodies at 15 hpi ($n = 5$; mean ± SD; two-way ANOVA, Sidak's multiple-comparison test). (H) Multicycle progeny production was monitored in L929 cells infected by T3wt or T3v10^{M1} at an MOI of 0.01. At indicated hours postinfection (hpi), we collected cell lysates and calculated PFU by plaque assay ($n = 3$; mean ± SD; two-way ANOVA, Sidak's multiple-comparison test). *, $P < 0.05$; **, $P < 0.01$; ***, $P < 0.001$; ****, $P < 0.0001$.

rather with later stages of reovirus replication, including transcription and virus factory formation. Accordingly, since our mission was to identify mutations in reovirus likely to promote postentry steps, we focused in subsequent analysis on determining the mechanism of increased plaque size by the reovirus monoreassortant containing only the A612V mutation in M1 (RA4/RA5). We renamed RA4 to T3v10^{M1}, generated plaque-

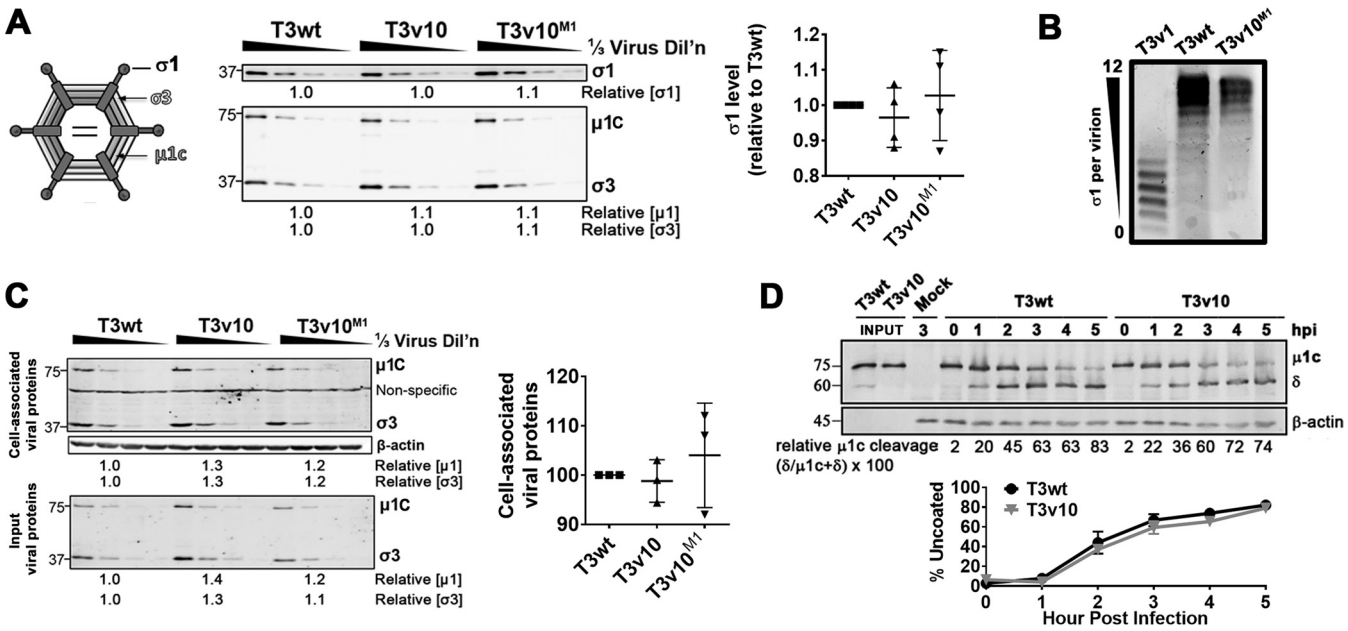

FIG 2 T3v10^{M1} has similar σ1 levels, binding, and uncoating as T3wt. (A) Equal particle amounts of cesium chloride (CsCl) gradient-purified T3wt, T3v10, and T3v10^{M1} were compared by Western blotting. Levels of σ1, μ1, and σ3 relative to those in T3wt are indicated. (Right) Results from 4 independent viral preparations are represented by dot plot ($n = 4$; mean ± SD, no significant differences). (B) Agarose gel electrophoresis of T3v1, T3wt, and T3v10^{M1} whole particles separated particles based on number of virion-associated σ1. (C) L929 cells were exposed to equivalent viral particles of T3wt, T3v10, and T3v10^{M1} for 1 h at 4°C. Unbound viruses were washed away with phosphate-buffered saline (PBS). Cell lysates were subjected to Western blot analysis. (Right) Cell-associated viral proteins were normalized to input viral proteins to calculate percentage of binding for multiple experiments ($n = 3$; mean ± SD, no significant differences). (D) Reovirus uncoating was monitored by Western blotting for cleavage of μ1c to δ. (Bottom) Line graphs represent percentage of uncoating at each indicated time point ($n = 3$; mean ± SD, no significant differences).

isolated stocks resequenced to be correct, and confirmed that T3v10^{M1} consistently produced larger plaques than T3wt (Fig. 1E).

We also generated the mutant T3v10^{M1} with a single mutation in μ2 (A612V) by reverse genetics (T3v10^{M1}-RG) and evaluated the plaque size generated in breast cancer cell lines. As expected, this mutant showed the same phenotype as the monoreassortant, an increased plaque size relative to T3wt in TUBO (mouse), T47D (human), and MCF7 (human) breast cancer cells (Fig. 1F).

To determine if T3v10^{M1} had advantages in a single round of replication, single-cycle growth kinetics were monitored at a high multiplicity of infection (MOI). One round of reovirus replication in L929 cells is completed at approximately 24 h postinfection. T3v10^{M1} produced an ~2.5-fold larger burst size than that of the T3wt per infected cell at 24 h-postinfection (hpi) (two-way analysis of variance [ANOVA]; $n = 5$, $P < 0.0001$) (Fig. 1G). In a multistep growth curve analysis, T3v10^{M1} accumulated 10-fold higher titers than T3wt by 48 hpi (two-way ANOVA; $n = 3$, $P = 0.0199$) (Fig. 1H). The A612V mutation in μ2 therefore provides an advantage in a single infectious cycle that is augmented over successive rounds of virus replication.

T3v10^{M1} has similar σ1 levels, binding, and uncoating to those of T3wt. As described in the introduction, it was previously discovered that genetic mutations in reovirus that reduce the levels of σ1 cell attachment proteins on reovirus particles increase reovirus uncoating efficiencies, increase plaque size on transformed cell lines, and improve oncolysis *in vivo* (17). T3v10^{M1} has a single amino acid replacement in the inner core protein μ2, which is unlikely to directly affect assembly of outer-capsid σ1 protein but could indirectly affect reovirus capsid conformation and thereby the incorporation of outer-capsid protein. Given that reduced σ1 levels on reovirions is an already known mechanism for increased plaque size, it was important to determine σ1 levels for T3v10^{M1}. The levels of σ1 trimers on cesium chloride (CsCl) gradient-purified T3wt, T3v10, and T3v10^{M1} virions were therefore assessed by quantitative Western blot analysis from three independent virus preparations (Fig. 2A). One-third dilutions of

virus particles were performed to obtain quantitative results and ensure subsaturation. Relative levels of σ1 were then compared to those of capsid proteins σ3 and μ1c. T3wt, T3v10, and T3v10^{M1} virions had similar ratios of σ1:σ3:μ1c, indicating that the three viruses had similar amounts of σ1 per virion. Agarose gel electrophoresis was performed to confirm Western blot analysis (Fig. 2B). According to a study by Larson et al. (42), reovirus can produce up to 12 bands that migrate at different speeds on agarose gel, depending on the quantity of virion-associated σ1. As expected, T3v1 produced species with faster migration since the virus possesses 3-fold less σ1 (on average) compared to T3wt, while T3wt and T3v10^{M1} species migrated similarly. These results indicate that mutations in S1 or M1 of T3v10 increase plaque size by mechanisms distinct from the previously described reduction in σ1 levels.

Since reduced σ1 level was not the mechanism for increased plaque size by T3v10^{M1} relative to T3wt, it was necessary to pinpoint the step of reovirus replication that was enhanced by the mutation in μ2 of T3v10^{M1}. Reovirus replication can be temporally segregated into entry versus postentry steps, where entry refers to attachment, endocytosis, and uncoating of input virions, while postentry steps include subsequent *de novo* synthesis and amplification of reovirus macromolecules. To determine if cell attachment was augmented for T3v10^{M1} relative to T3wt, a binding assay was performed. L929 cells were subjected to serial dilutions of T3wt, T3v10, and T3v10^{M1} at 4°C to permit virus-cell association without entry (Fig. 2C). Following excessive washing to remove unbound virions, Western blot analysis for reovirus structural proteins was performed to quantify the proportion of cell association virions. All three viruses showed similar binding to L929 cells, which was not surprising given that they contain similar amounts of the cell attachment protein σ1.

Following cell binding and endocytosis, reovirus undergoes uncoating in endolysosomes with the aid of proteases such as cathepsins B, S, and L (43–45). Uncoating of reovirus requires complete degradation of outer capsid protein σ3 and cleavage of underlying μ1C to the δ fragment. Particles bearing the δ fragment, referred to as infectious subviral particles (ISVPs), are capable of penetrating membranes to deliver fully uncoated and transcriptionally active core particles to the cellular cytoplasm (2, 46–48). To monitor uncoating rates for T3v10 versus T3wt, L929 cells were exposed to these viruses at 37°C to permit binding and entry, and lysates were monitored hourly for the hallmark cleavage of μ1C to the δ by Western blotting (Fig. 2D). The percentage of virion uncoating (δ/δ plus μ1C) was similar for T3wt and T3v10 over three independent experiments, indicating that the mutation in T3v10 did not support enhanced uncoating rates. Given that the parental T3v10 did not show improved uncoating over wild-type reovirus, there was no incentive to perform uncoating kinetic analysis for subvariant T3v10^{M1}. Overall, attachment and uncoating could not account for differences in replication between T3wt and T3v10, revealing T3v10 as the first mutant of T3wt to exhibit enhanced proliferation in transformed cells owing to postentry steps of replication.

Paradoxically, T3v10^{M1} is impaired in hydrolyzing ribonucleoside triphosphates and RNA synthesis *in vitro*. The μ2 protein is a structural protein of the inner core, juxtaposed to the polymerase λ3 (49, 50). The purified μ2 protein alone possesses both RNA 5′-triphosphatases (RTPases) and nucleoside-triphosphatase (NTPase) activities that are mildly enhanced by inclusion of λ3; therefore, μ2 is considered a polymerase cofactor (20). We sought to determine if the A612V mutation in μ2 of T3v10^{M1} impacts μ2 triphosphatase activities by performing ribonucleoside triphosphate (rNTP) hydrolysis assays using μ2-bearing viral cores. To obtain viral cores, equivalent numbers of particles of T3wt or T3v10^{M1} were incubated with the proteolytic enzyme chymotrypsin (CHT) until the outer capsid proteins were completely digested, followed by high-speed ultracentrifugation to purify cores, a procedure well established for reovirus to produce transcriptionally active core particles (51). Successful conversion of full virions to cores was confirmed by depletion of outer capsid protein μ1c, σ3, and σ1 from particles (Fig. 3A). To measure NTPase activities, cores were incubated with rATP, rGTP, rCTP, or rUTP in separate reactions, and release of phosphate ions was measured by a

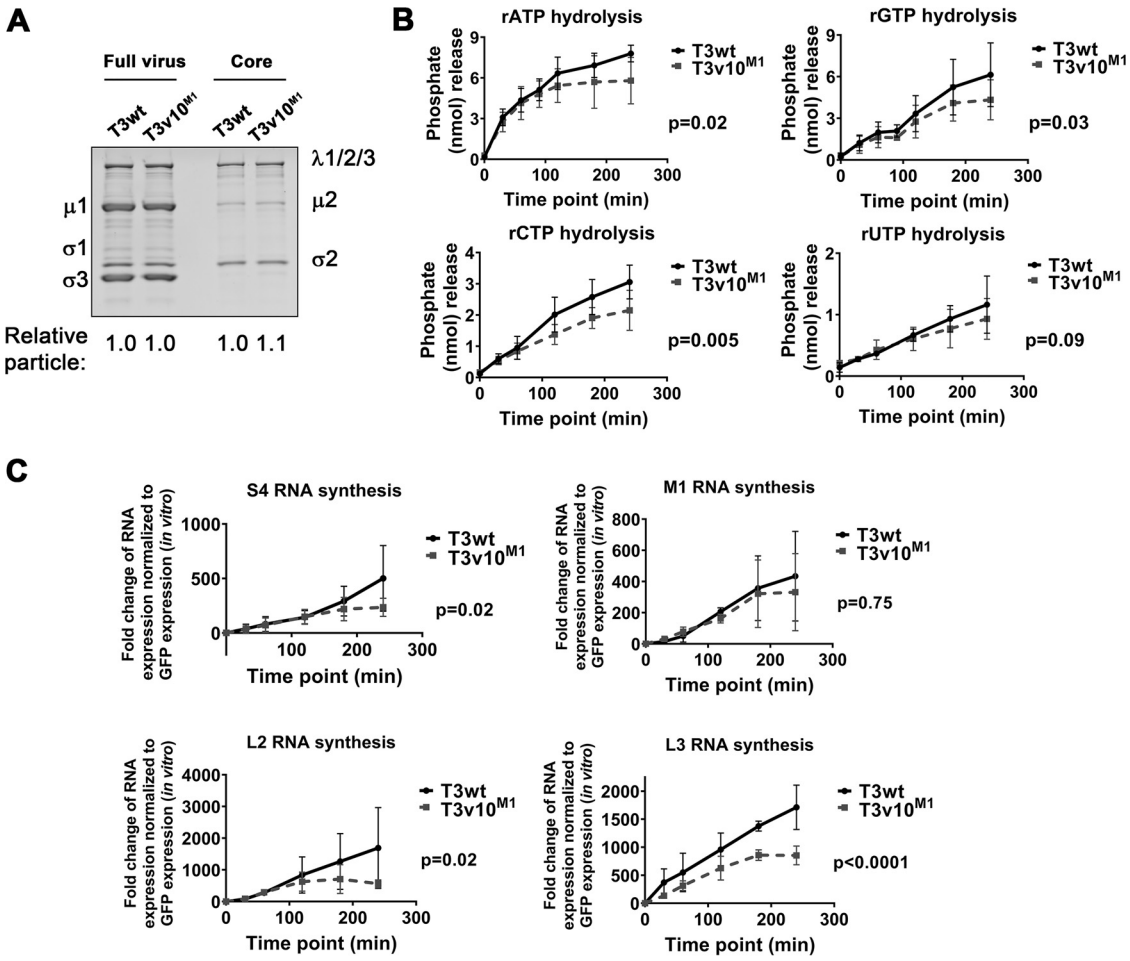

FIG 3 T3v10^{M1} is impaired in hydrolyzing ribonucleoside triphosphates (rNTPs) and RNA synthesis *in vitro*. (A) Equivalent amounts of T3wt and T3v10^{M1} full virions were digested by chymotrypsin (CHT) to obtain μ2-bearing viral cores. Coomassie blue staining confirmed removal of outer capsid proteins. (B) T3wt and T3v10^{M1} viral cores were incubated with rNTPs at 37°C. Hydrolysis of rNTPs by T3wt or T3v10^{M1} μ2 was determined by the formation of chromogenic complex when phosphate ions reacted with colorimetric reagents ($n = 4$; mean ± SD; nonlinear regression analysis), and (C) *in vitro* synthesis of viral RNAs was measured by quantitative reverse transcription-PCR (RT-qPCR) ($n = 3$ for S1, M1, and L2 RNA synthesis; $n = 4$ for L3 RNA synthesis; mean ± SD; nonlinear regression analysis).

colorimetric phosphate assay kit. Surprisingly, nonlinear regression analyses revealed that T3v10^{M1} was ~2-fold slower at hydrolyzing rATP, rGTP, and rCTP compared to T3wt (Fig. 3B). Furthermore, hydrolysis of rATP and rGTP by viral cores of T3v10^{M1} plateaued at the 120- to 180-minute time point, while T3wt continued to hydrolyze all 4 rNTPs up to the final 240-minute time point. Previous studies showed that enzymatic activities of μ2 are affected by pH and temperature *in vitro* (21); however, we obtained similar results at pH 7.0 and temperatures of 37°C (Fig. 3B) and 40°C (data not shown). Therefore, although we initially set out to identify an advantage of the A612V μ2 mutation that conferred larger plaques, paradoxically, rNTP hydrolysis analysis suggested that the A612V μ2 mutation contrarily confers a disadvantage with respect to nucleotide processing.

Although evidence for μ2 rNTPase activities was previously described and inferred to have a role in transcription, a direct relationship between μ2-mediated NTPase activity and λ3-mediated RNA synthesis has not yet been confirmed. The reduced rNTPase activities of T3v10^{M1} provided an opportunity to test the relationship of μ2 rNTPase activities with core transcription. To measure RNA synthesis *in vitro*, viral cores were incubated with substrates for RNA synthesis, and accumulation of reovirus RNAs was monitored by quantitative reverse transcription-PCR (RT-qPCR). Reovirus has 10 genes that fall into three size classes, small (S), medium (M), and large (L). S4, M1, L2,

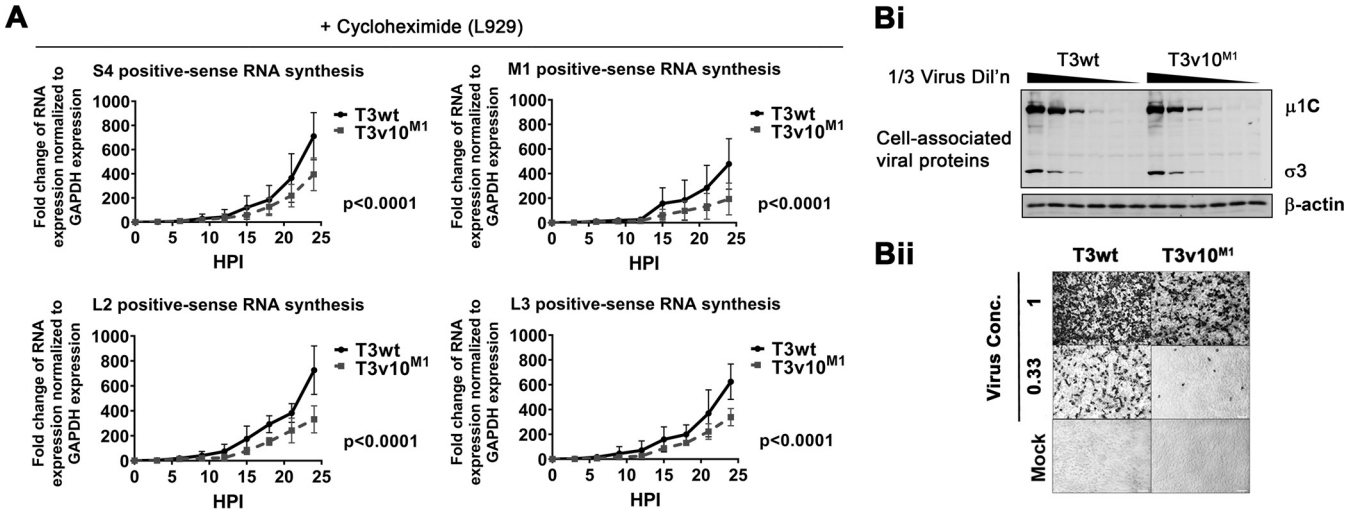

FIG 4 In cells, T3v10^{M1} has impaired RNA synthesis and has reduced probability of establishing productive infection. (A) L929 cells were exposed to equivalent amounts of T3wt and T3v10^{M1} cell-bound virions in the presence of CHX. Synthesis of 4 representative positive-sense RNAs were compared between the two viruses ($n = 4$; mean ± SD; nonlinear regression). (B) (i) L929 cells were exposed to equal amounts of cell bound T3wt and T3v10^{M1}, as confirmed by Western blotting. (ii) Immunocytochemical staining shows that for the same number of cell-bound particles assessed in subpanel i, T3v10^{M1} results in fewer productively infected cells relative to T3wt. Cells were fixed at 18 hpi and subjected to immunohistochemistry (IHC) with polyclonal antireovirus antibodies.

and L3 were chosen as representative genes of each size class for RT-qPCR analysis. Nonlinear regression analyses indicated that T3v10^{M1} produced viral RNAs at a lower rate than T3wt (Fig. 3C). Moreover, RNA synthesis plateaued for T3v10^{M1} by 120 to 180 min, while RNA synthesis continued up to the last 240-minute time point for T3wt. Results from the *in vitro* transcription assay (Fig. 3C) versus the rNTP hydrolysis assay (Fig. 3B) were strikingly similar; the current study therefore provides evidence to support the hypothesis that $\mu 2$ plays a direct role in the process of RNA synthesis.

In cells, T3v10^{M1} has impaired RNA synthesis and has a reduced probability of establishing productive infection. T3v10^{M1} synthesized RNAs at lower rates than T3wt *in vitro*, but whether T3v10^{M1} exhibited the same behavior in cells remained to be elucidated. To assess reovirus core transcription during cell infection, it became essential to inhibit posttranscription steps of virus replication and prevent potential confounding effects of virus amplification. Specifically, reovirus transcription occurs in two phases. During the primary phase of transcription, incoming virions uncoat to cores that transcribe and release positive-sense viral RNAs [(+)RNAs] into the cytoplasm. Some (+)RNAs become templates for viral protein synthesis, while others become encapsidated into progeny cores. Progeny cores synthesize negative-sense RNAs [(−)RNAs] within them, and then, importantly, contribute more (+)RNAs to the cytoplasm in a process called the secondary phase of transcription. Accordingly, to study reovirus core RNA synthesis in isolation, it was imperative to stop subsequent steps of protein synthesis and progeny core assembly, as these steps could have indirect effects on viral RNA accumulation.

To perform in-cell core transcription assessment, we therefore treated L929 cells with cycloheximide (CHX) to inhibit protein expression and used RT-qPCR to monitor viral RNA synthesis of only incoming T3wt and T3v10^{M1} virions. Western blot analysis verified that CHX treatment completely inhibited synthesis of viral proteins (data not shown). Reovirus-infected cells were collected at 3-h intervals over a 24-h period and subjected to RNA purification and RT-qPCR analysis for viral RNAs relative to cellular GAPDH. To distinguish (+)RNAs and (−)RNAs, sense-specific primers were used during the reverse transcription reaction. Both T3wt and T3v10^{M1} were able to synthesize (+) RNAs (Fig. 4A), with the normalized fold changes of RNA synthesis recapitulating the *in vitro* transcription assay (Fig. 3C). Importantly, nonlinear regression analysis indicated that T3wt produced (+)RNAs at about 2-fold higher rates than T3v10^{M1} for all tested

genes, and the differences were statistically significant. Negative-sense RNAs were not detected during infection (data not shown), which was anticipated given that CHX prevents protein expression and therefore progeny cores. Together, the data consistently showed that T3v10^{M1} was less effective at RNA synthesis *in vitro* and in cells. As extrapolated in the Discussion, although the C-terminal loop in μ2 that houses the A612V mutation was previously hypothesized to partake in polymerase cofactor functions based on structural proximity, the findings we present here provide the first empirical support for the function of this μ2 loop *in vitro* and in cells.

Given the deficiencies in RNA synthesis exhibited by T3v10^{M1}, we next compared the ability of T3v10^{M1} to establish productive infection relative to T3wt. First, we equalized T3wt and T3v10^{M1} doses to generate the same number of cell-bound virus particles by Western blotting (Fig. 4B, subpanel i). L929 cells exposed to equivalent cell-bound T3wt or T3v10^{M1} particles were then subjected to immunocytochemical staining at 18 hpi with polyclonal antireovirus antibodies (Figure 4B, subpanel ii). T3wt produced ~3-fold higher numbers of reovirus protein-expressing cells relative to T3v10^{M1}. Given that T3v10^{M1} produced fewer initially infected cells that T3wt, but generated a larger burst size and larger plaques, the results suggested that the disadvantages in NTPase activity and RNA synthesis were likely overcome by a separate advantage at posttranscription stages of reovirus replication.

Cells productively infected by T3v10^{M1} accumulate higher levels of viral RNAs and proteins over the course of infection relative to T3wt. To determine if T3v10^{M1} acquired advantages at the posttranscription stages of virus replication, we directly assessed viral RNA and protein synthesis over the course of infection. In these experiments, it was essential to omit CHX and permit normal virus amplification. To monitor RNA accumulation, L929 cells were exposed to equivalent amounts of cell-bound T3v10^{M1} and T3wt virions. RNA from total cell lysates was collected every 3 h in a 24-h period. RT-qPCR analysis was performed to monitor positive- and negative-sense RNA synthesis. Starting at approximately 9 hpi, which corresponds to midamplification in the secondary phase of transcription, rates of RNA synthesis became at least 2-fold higher for T3v10^{M1} relative to T3wt (Fig. 5A). Although total levels of viral RNAs fluctuate between experiments, nonlinear regression analyses suggested the differences in line slopes were significant for all tested genes. Synthesis of negative-sense RNA syntheses resembled (+)RNA synthesis between the two viruses (Fig. 5B). Most striking is that T3wt transcription tended to plateau at 15to 18 hpi as normally seen for this virus, while T3v10^{M1} exhibited a longer RNA production period. We also noticed that RNA synthesis of M1 gene seems less affected in T3v10^{M1} relative to other genes, and the same trend was observed in Fig. 5A. Although we cannot explain this phenomenon currently, it would be interesting in future to explore if discrimination exists between reovirus segments during transcription.

In congruence with higher accumulation of viral RNAs, accumulation of viral proteins was also enhanced in cells productively infected by T3v10^{M1} relative to T3wt. By Western blotting at 12 hpi and 15 hpi, virus proteins μ1, σ3, and μ2 were 2- to 4-fold higher for T3v10^{M1} than for T3wt and were standardized to β-actin (Fig. 5C; left is a representative blot for 3 matched virus dilutions and right is analysis of 3 independent experiments). That 12 hpi shows larger differences in relative μ1 and σ3 protein expression than 15 hpi may reflect that exponential growth of virus starts to taper at 12 to 15 hpi and becomes saturated. It is interesting that μ2 protein expression does not become saturated by 15 hpi and retains a 3-fold difference in expression at both time points; whether the fate of M1/μ2 expression is distinct from that of other viral proteins would be interesting to explore in future. Overall, bulk viral RNA and proteins are higher for T3v10^{M1} than for T3wt during secondary phase of replication (>9 hpi).

When infection doses were matched to produce equivalent numbers of infected cells, it was easy to visualize by flow cytometry that the histogram peak, representing cells positively stained by polyclonal antireovirus antibodies, exhibits higher mean fluorescence intensity at 15 hpi for T3v10^{M1} relative to T3wt, indicating higher overall levels of viral proteins per infected cell (Fig. 5D). Thus, despite the fact that T3v10^{M1}

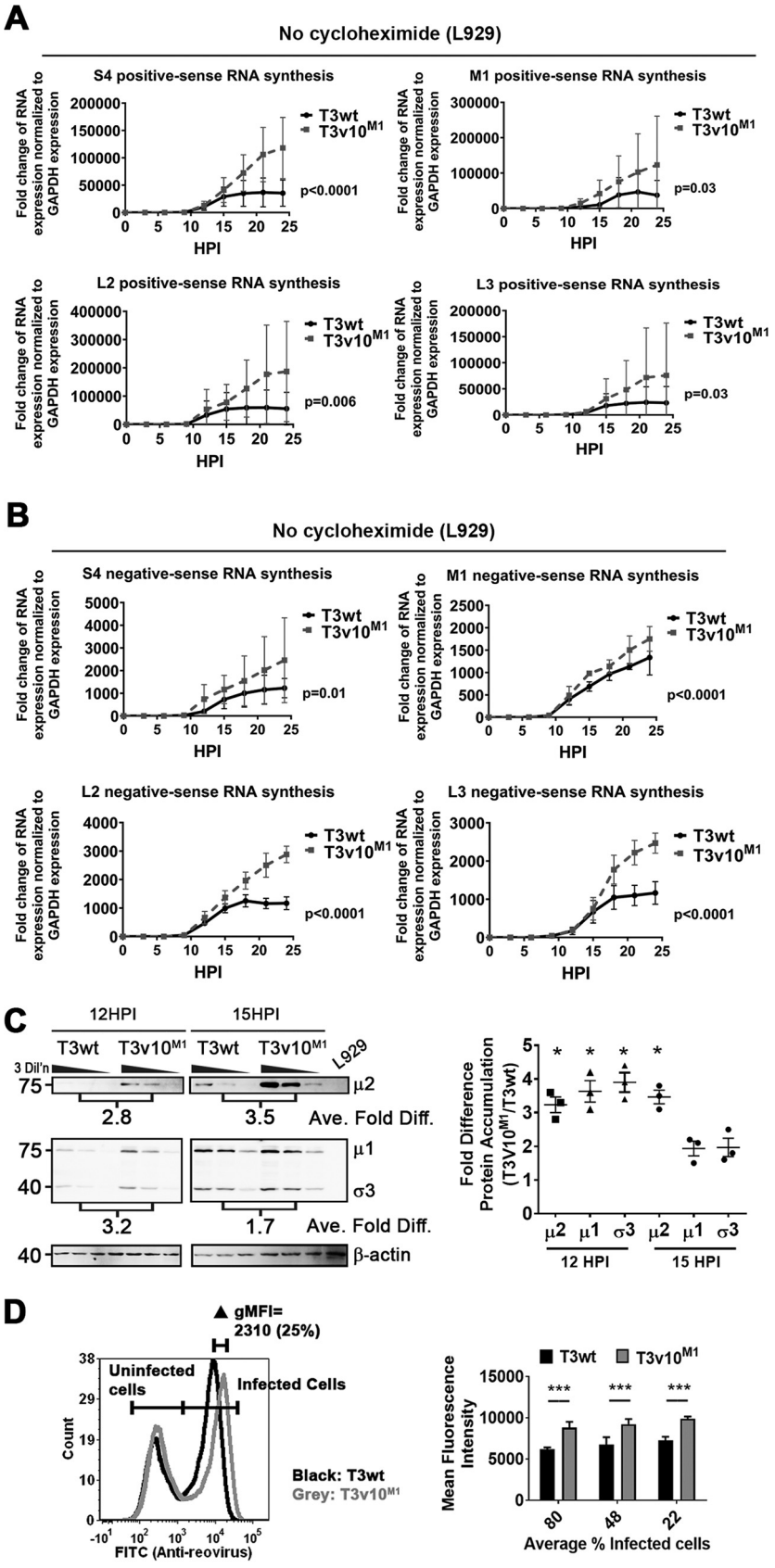

FIG 5 Cells productively infected by T3v10^{M1} accumulate higher levels of viral RNAs and proteins over the course of infection relative to those infected by T3wt. (A) Positive-sense RNA and, (B) negative-

(Continued on next page)

initially struggles to establish infection due to hampered NTPase activity and RNA synthesis, the fate of infection by T3v10^{M1} is reversed during the secondary phase of transcription, in which T3v10^{M1} achieves higher accumulation of viral RNAs and proteins.

T3v10^{M1} μ2 has increased association with μNS compared to T3wt μ2. In addition to its role as a polymerase cofactor within cores, soluble μ2 produced during infection plays a secondary function, namely, it supports the formation of localized sites for virus amplification and assembly called viral factories (31, 35). To facilitate factory formation, μ2 tethers the nonstructural viral protein μNS to microtubules, and μNS in turn recruits other viral proteins (31, 52). μNS also binds the viral nonstructural protein σNS, which associates with RNAs (53).

Given that viral factory formation directly affects reovirus replication and that μ2-μNS cooperation is needed to assemble the viral factory properly, we wondered if the A612V mutation in μ2 might affect association with μNS, and we therefore developed assays to quantify μ2-μNS interactions. First, coimmunoprecipitation (Co-IP) was performed on lysates of L929 cells infected with T3v10^{M1} or T3wt (Fig. 6A). To account for differences in establishing infection and *de novo* protein expression, cell infections were standardized to produce equivalent virus protein levels between the two viruses, as confirmed by Western blotting (Fig. 6A). When anti-μ2 antibodies were used to pull down μ2 and proteins that associated with μ2, Western blot analysis revealed that ~9-fold more μNS was coprecipitated with T3v10^{M1} μ2 than with T3wt μ2.

Coassociation between μ2 and μNS during virus infection does not imply direct interactions, since these proteins could interact through an intermediate complex. To focus on μ2-μNS associations independently of other viral factors, we developed Far Western blotting to investigate direct μ2 and μNS interactions (Fig. 6B). Since L929 cells are poorly transfectable, the reovirus-permissive and easily transfected H1299 lung carcinoma cell line was used. H1299 cells were transfected with μNS alone, N-terminally Flag-tagged μ2 with wt or T3v10^{M1} (10^{M1}) sequence, or Flag-tagged dengue virus capsid protein (NS1) as a negative control. In addition, we had His-tagged wild-type μNS (purified μNS) and μ2 (purified μ2) that were previously purified from bacterial expression systems, which we included during electrophoresis as additional controls. Three serial dilutions of each lysate, alongside the two purified proteins, were subjected to nondenaturing gel electrophoresis to preserve native protein structure, and then transferred to polyvinylidene difluoride (PVDF) membranes. Direct Western blot analysis with Flag-specific antibodies showed that wild-type μ2 and T3v10^{M1} μ2 were present at similar levels (Fig. 6C and D, bottom anti-Flag blot). The specificity of Flag and μNS antibodies was evident from μNS-only-transfected and Flag-NS1-transfected controls. Far-Western blot analysis was then performed with either lysates of H1299 cells transfected with μNS (Fig. 6C) or purified μNS (Fig. 6D), followed by the detection of associated μNS using rabbit μNS-specific antibodies. Under both conditions and over 5 independent experiments, ~2-fold more μNS associated with T3v10^{M1} μ2 than with wild-type μ2 (Fig. 6E). The μ2-μNS interaction was specific, because Flag-tagged NS1 did not interact with μNS. Furthermore, μ2 did not self-associate after the PVDF membrane was incubated with purified His-μ2 (data not shown). Far-Western blotting suggested that T3v10^{M1} μ2 had a stronger direct association with μNS.

FIG 5 Legend (Continued)
sense RNA syntheses were compared between T3wt and T3v10^{M1} in L929 cells by RT-qPCR ($n = 4$; mean ± SD; nonlinear regression). (C) Equivalent amounts of L929 cells were infected by T3wt or T3v10^{M1}. Total cell lysates were subjected to Western blot analysis, and intensities of protein bands were quantified by ImageQuant 1D gel analysis software. (Right) Fold difference of protein accumulation (T3v10^{M1}/T3wt) for multiple experiments summarized by dot plot ($n = 3$; mean ± SD; one-sample *t* test comparing fold difference to the theoretical mean of 1). (D) Left, histogram from flow cytometry analysis comparing mean fluorescence intensity (MFI) of T3wt- and T3v10^{M1}-infected L929 cells. Reovirus antigen-positive cell population (right peak) represents virally infected cells. Right, L929 cells were infected with different doses of T3wt or T3v10^{M1}, and MFIs are compared by bar graphs ($n = 3$; mean ± SD; two-way ANOVA with Dunnett's multiple-comparison test). *, $P < 0.05$; **, $P < 0.01$; ***, $P < 0.001$; ****, $P < 0.0001$.

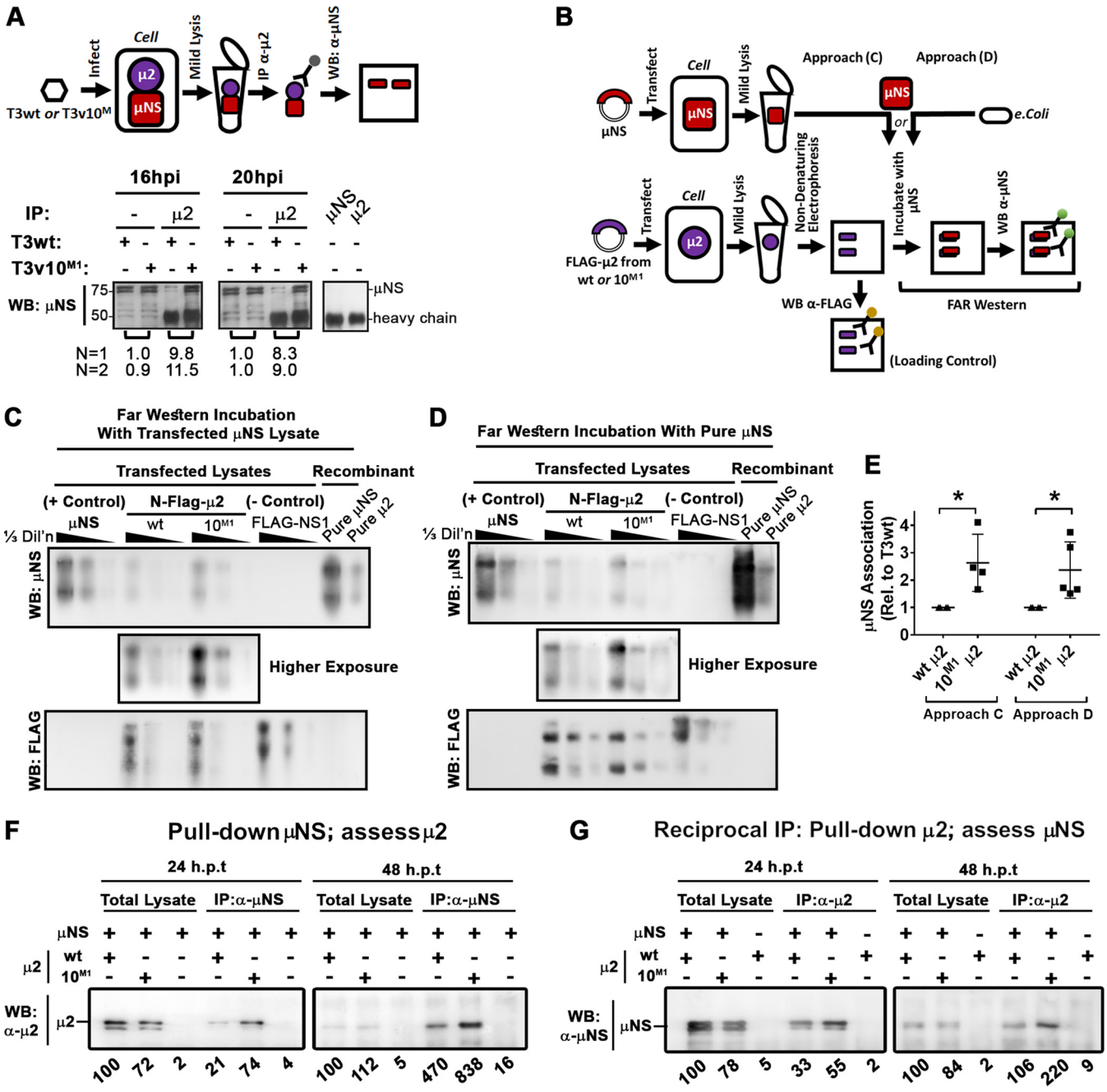

FIG 6 T3v10^{M1} μ2 has increased association with μNS relative to T3wt μ2. (A) L929 cells were infected with T3wt or T3v10^{M1}. Whole-cell lysates were collected at the indicated time points, and μ2 was immunoprecipitated by antibodies specified in the figure. Western blot analysis with anti-μNS was then conducted to evaluate μNS coimmunoprecipitated with μ2. Densitometric analysis for two independent experiments ($N = 1$ being the representative image presented) of μNS in T3v10^{M1} relative to T3wt for matched pairs is provided. (B) Schematic of experimental procedure for the far-Western blot analyses in panels C and D. H1299 cells were transfected with serially diluted plasmids expressing wild-type (wt) μ2 or μ2 derived from T3v10^{M1} (10^{M1}). All μ2 proteins had a 5′ terminal Flag tag. H1299 cells were harvested in a mild lysis buffer 24 h posttransfection. Total cell lysates were subjected to polyacrylamide gel electrophoresis. Proteins were transferred to polyvinylidene difluoride (PDVF) membranes, following by incubation with PBS containing (C) cell lysate transfected with μNS or (D) purified μNS from *Escherichia coli*. For panels C and D, NS1 was a Flag-tagged Dengue virus capsid protein included as a negative control. μNS and μ2 proteins purified from *E. coli*. (right 2 lanes) were loaded as positive controls. Finally, Western blot analysis with anti-Flag shows the levels of Flag-tagged proteins on the membrane, while Western blot analysis with anti-μNS shows the levels of μNS that associated with the μ2 proteins on the membranes. (E) Results from 4 independent far-Western blot experiments are represented in dot plots (mean ± SD; paired *t* test). (F and G) Coimmunoprecipitation was also conducted to measure association between μNS and μ2. H1299 cells were cotransfected with μNS and Flag-tagged wild-type (wt) μ2 or Flag-tagged μ2 derived from T3v10^{M1} (10^{M1}). Whole-cell lysates were harvested 24 h posttransfection (hpt). Immunoprecipitation was performed using (F) anti-μNS (α-μNS) or (G) anti-μ2. Western blot analysis was then conducted with (F) anti-μ2 (α-μ2) or (G) anti-μNS (α-μNS). Relative levels of μ2 coprecipitated with μNS (F), or reciprocally, μNS coprecipitated with μ2, are provided below the corresponding lanes. *, $P < 0.05$; **, $P < 0.01$; ***, $P < 0.001$; ****, $P < 0.0001$.

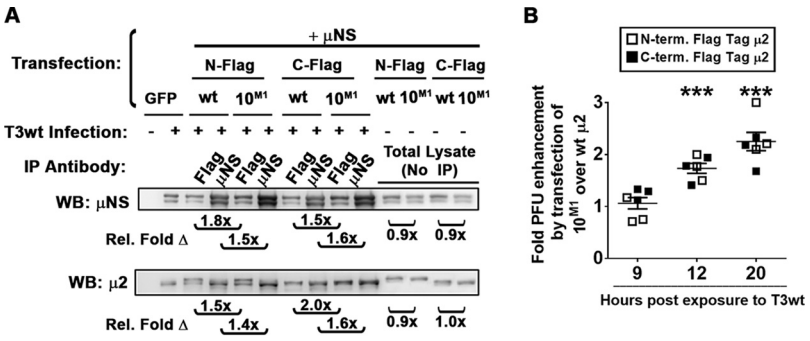

FIG 7 Cotransfection of μNS and T3v10^{M1} μ2 promotes progeny production. (A) H1299 cells were cotransfected with μNS and wild-type (wt) μ2 or μ2 derived from T3v10^{M1} (10^{M1}). The μ2 were either C- or N-terminally Flag-tagged as indicated. At 24 h posttransfection, cells were infected at an MOI of 3 with T3wt, and whole-cell lysates were harvested at 12 h postinfection. Immunoprecipitation was performed using anti-μNS or anti-Flag, as indicated. Western blot analysis was then conducted with anti-μ2 or anti-μNS (α-μNS). Relative levels of Flag-μ2 coprecipitated with μNS, or reciprocally, μNS coprecipitated with Flag-μ2, are provided below the corresponding lanes. Protein band intensities were quantified by ImageQuant. (B) H1299 cells were transfected with a plasmid expressing either an N- or C-terminal Flag-tagged μ2 derived from T3wt or from T3v10^{M1} (10^{M1}). After 24 h of transfection, cells were infected with T3wt at an MOI of 4. At 9, 12, and 20 hpi, whole-cell lysates were frozen and thawed three times and subjected to plaque titration. Data are presented as the ratio of infectious virus (PFU) from T3wt-infected cells transfected by 10^{M1}-derived μ2 over T3wt-infected cells transfected with T3wt-derived μ2 (mean $\pm$ SD; one-sample *t* test comparing sample mean to theoretical mean of 1). *, $P < 0.05$; **, $P < 0.01$; ***, $P < 0.001$; ****, $P < 0.0001$.

As a complementary approach to assess direct μ2-μNS interaction, H1299 cells were transfected for 24 or 48 h with μNS and Flag-tagged μ2 derived from T3wt or T3v10^{M1} and subjected to coimmunoprecipitation analysis. Transfected cell lysates were either loaded for Western blot analysis (total lysates) to monitor total protein levels or immunoprecipitated with μNS-specific antibodies prior to Western blot analysis for coassociated μ2 (Fig. 6F). At both time points, ~2-fold more T3v10^{M1} μ2 than wt μ2 protein coassociated with μNS. In reciprocal co-IP (Fig. 6G), ~2-fold more μNS was pulled down with μ2-specific antibodies when μ2 was derived from T3v10^{M1} than with that derived from T3wt. The transfection in cell co-IP (Fig. 6F and G) corroborated with far-Western blotting results (Fig. 6C to E) to suggest that the A612V mutation in μ2 enhances direct μ2-μNS associations, which are further augmented during virus infection (Fig. 6A).

Cotransfection of μNS and T3v10^{M1} μ2 promotes progeny production. Results thus far showed that μ2 from T3v10^{M1} increases postentry stages of replication during virus infection, and independently that plasmid-derived μ2 from T3v10^{M1} associates more with μNS. The final question was whether these two processes are likely to be connected and, in other words, whether plasmid-derived Flag-tagged μ2 with an A612V mutation could increase progeny production during infection by T3wt. To account for possible occlusion by the Flag tag, we also generated C-terminally Flag-tagged μ2 proteins from T3v10^{M1} and T3wt. H1299 cells were transfected with μNS and μ2 proteins (C- or N-tagged from T3v10^{M1} or T3wt as indicated), but then infected with T3wt. Co-IP experiments similar to those shown in Fig. 6F and G were first repeated in the context of these new transfection-infection experiments and corroborated that Flag-tagged μ2 proteins have stronger associations with μNS when derived from T3v10^{M1} than when derived from T3wt (Fig. 7A). It is important to notice here that the N-terminal tags slowed down the μ2 mobility migration, and this is why when we also infected with T3wt we detected two bands, the first one from the transfected μ2 (N-flag) and the lower band from the virus infection. Finally, we determined the effect of transfected μ2 proteins on progeny production during T3wt infection. Specifically, we compared titers from T3wt-infected cells transfected with T3v10^{M1}-derived versus T3wt-derived μ2. At 9 hpi, there was no difference between the μ2 proteins, but at 12 and 20 hpi, T3v10^{M1} -derived μ2 increased viral titers ~2-fold

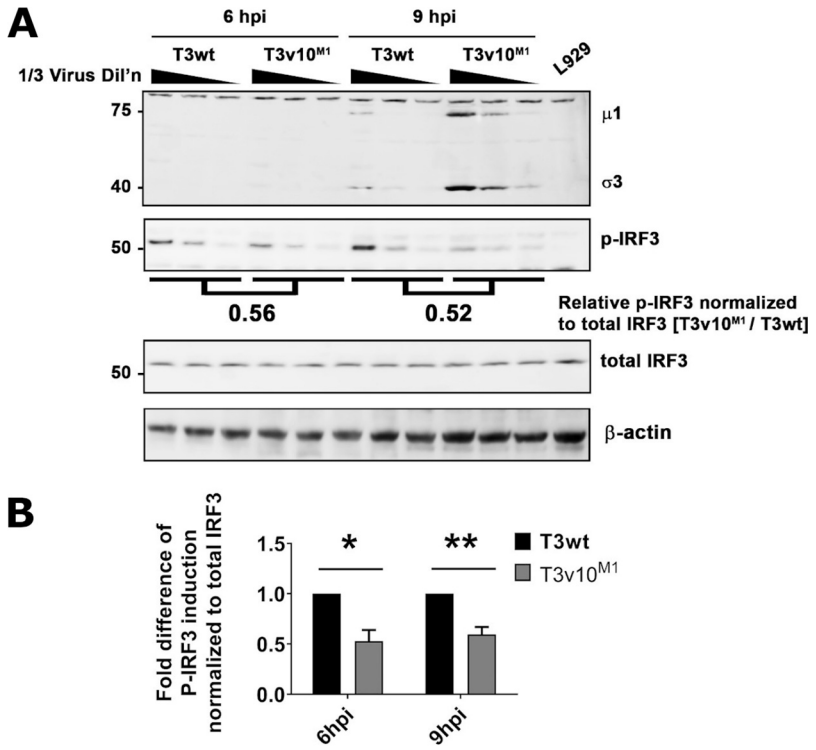

FIG 8 T3v10^{M1} infection reduces levels of IRF-3 phosphorylation compared to that by T3wt. (A) L929 cells were exposed to T3wt or T3v10^{M1}at a viral dose to infect 70% of the cells, which was confirmed by flow cytometry. Cell lysates were collected at 6 and 9 hpi. Total levels of IRF3 and phosphorylated (active form) IRF3 were determined by Western blotting. (B) Quantification of IRF3 activation. Levels of phosphorylated IRF3 (p-IRF3) were normalized to total IRF3. Three independent experiments were performed and graphed (mean ± SD; two-way ANOVA with Dunnett's multiple-comparison test). *, $P < 0.05$; **, $P < 0.01$; ***, $P < 0.001$; ****, $P < 0.0001$.

compared to T3wt μ2 (Fig. 7B; $P < 0.05$). Both C- and N-terminal Flag-tagged μ2 constructs behaved similarly. The data support previous studies implicating μ2-μNS interaction as an important factor for virus replication, but for the first time, we show that such interaction is not saturated in T3wt and can be augmented to promote replication in transformed cells. As discussed further below, these are the first studies to implicate the C-terminal loop of μ2 in μ2-μNS, which is surprising given that previously described μ2-μNS domains are distal from A612V.

Inhibition of antiviral response is an additional benefit of T3v10^{M1} infection. Another described function of μ2 is its role affecting cellular innate antiviral response. For example, the μ2-encoding M1 gene is a determinant of interferon (IFN) signaling and myocarditis in neonatal mice (54, 55). Moreover, reovirus factories produced by μNS and μ2 were discovered to sequester and inhibit interferon regulatory factor 3 (IRF3) (56). Considering that μ2 and μNS can affect the antiviral immune response, we evaluated if the A612V mutation affected IRF3 phosphorylation as a routine measure of IRF3 activation. T3v10^{M1} consistently induced lower levels of phosphorylated IRF3 (p-IRF3) relative to T3wt at 6 and 9 hpi, despite the fact that more viral proteins were synthesized from the T3v10^{M1}-infected cells (Fig. 8A and B). These results are consistent with two scenarios, as follows: (i) given published evidence that μNS sequesters IRF3 into viral factories (56), the A612V μ2 mutation and enhanced μ2-μNS interactions could promote IRF3 sequestration, or (ii) given published evidence that the faster-replicating T3D^{PL} strain causes less p-IRF3 than the slower-replicating T3D^{TD} strain and T3D^{TD}/T3D^{PL} reassortants (57), the A612V μ2 mutation might allow less time for IRF3 induction by merely increasing viral macromolecular synthesis and virus "concealment" abilities. Importantly, however, published data strongly indicate that IFN production does not affect the first round of replication for reovirus (57), and hence the decreased

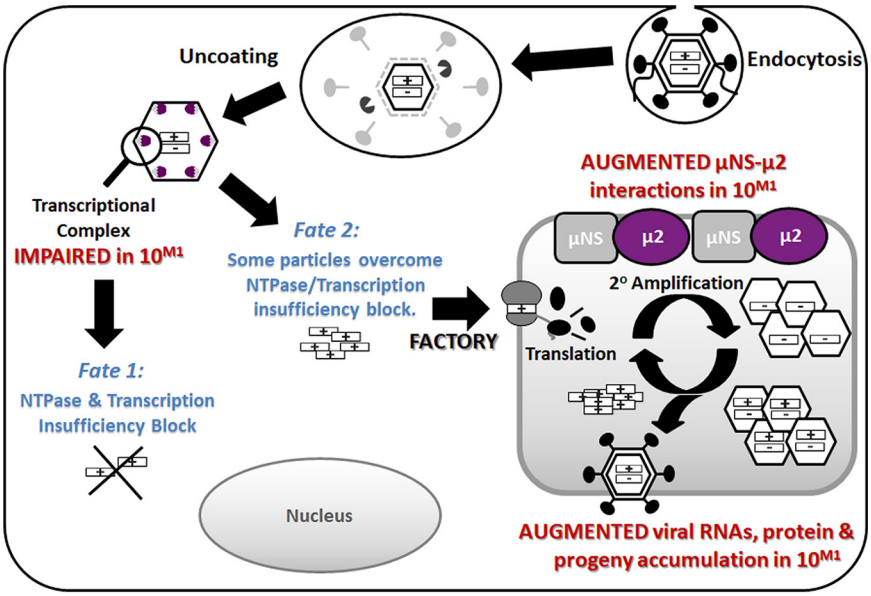

FIG 9 Final model. Reovirus variant T3v10^{M1} has a single amino acid alteration, A612V, in the previously uncharacterized C-terminal loop of μ2. The alteration does not change the levels of cell attachment protein σ1, and therefore it binds and uncoats in a similar manner to that of T3wt. As a polymerase cofactor and a major part of the transcriptional complex (λ3-μ2), the single-residue replacement impairs NTPase activities and RNA synthesis and causes ~80% of virions to fail to initiate productive infection (producing detectable viral proteins) (fate 1). However, for the T3v10^{M1} virus particles that are capable of overcoming the transcriptional limitations, T3v10^{M1} μ2 produces increased associations with μNS and promotes progeny synthesis (fate 2). Overall, the A612V mutation in μ2 produces a negative impact (fate 1) and a positive impact (fate 2) on distinct stages of virus replication, but the net sum of these fates is beneficial, as indicated by increased plaque size and burst size in virus growth curves.

IRF3-P by T3v10 ^{M1} is not the cause of increased levels of T3v10^{M1} RNA (Fig. 5A and B), proteins (Fig. 3C and D), and progeny (Fig. 1G) in the first 24 hpi. Still, less IRF3 activation could certainly affect subsequent rounds of reovirus infection of neighboring IFN-stimulated cells and contribute to the difference in plaque size (Fig. 1A to F).

DISCUSSION

Using directed evolution, we successfully identified T3v10^{M1} as the first reovirus variant with enhanced infectivity in cancer cells compared to that of T3wt due to advantages at postentry steps of replication. Subsequent experiments revealed that an A612V mutation in μ2 of T3v10^{M1} comes with both benefits and costs to virus fitness (model depicted in Fig. 9). These data are consistent with a role for the previously uncharacterized C-terminal region in transcription by incoming reovirus cores; specifically, T3v10^{M1} had 2- to 3-fold reduced NTPase and transcription processivity relative to those of T3wt *in vitro* (Fig. 3) and produced ~2-fold less RNA per input virion in L929 cells when cycloheximide was added to preclude secondary rounds of replication (Fig. 4A). The reduced transcription created a "cost," a 2- to 3-fold decrease in the number of cells that became productively infected with T3v10^{M1} (Fig. 4B). Conversely, the A612V mutation in μ2 of T3v10^{M1} brought a postentry benefit as well. T3v10^{M1} particles that did successfully establish infection produced 2- to 3-fold higher levels of viral RNA (Fig. 5A and B), viral proteins (Fig. 5C to E), and progeny (Fig. 1G and H) relative to those of T3wt. The A612V mutation in μ2 led to enhanced interaction between μ2 and both μNS and tubulin (Fig. 6). Moreover, plasmid-derived μ2 containing the A612V mutation associated better with μNS and was sufficient to increase progeny production by T3wt (Fig. 7). Finally, we showed that the A612V mutation also decreased cellular antiviral immune response (Fig. 8). Together, the data implicate the C-terminal loop of μ2 in the transcription of incoming cores, μNS association of *de*

novo virus proteins, and antiviral signaling. The net costs and benefits of the A612V mutation produced an overall 2-fold enhancement of replication relative to that of T3wt in growth curves, and overall larger plaque size.

Effects of the μ2 C-terminal domain on NTP hydrolysis and transcription. In the absence of crystal structures for mammalian orthoreovirus (MRV) μ2, we turned to a recently published structural model of VP5 (the *Aquareovirus* homolog of μ2) to deduce how the A612V alteration could affect NTPase activities (49). Previous studies identified two putative nucleoside triphosphate (NTP)-binding motifs (KxxxK and SDxxG) that are widely conserved in different genera and subspecies of *Reoviridae*, despite the length of μ2 sequences differing remarkably (22, 23). Among all subspecies of *Reoviridae*, *Aquareovirus* VP5 is the most homologous to the MRV μ2, and the VP5 is only 8 residues shorter than MRV μ2. The NTP-binding motifs are found between residues 400 and 450 in both VP5 and μ2 (23). Based on the linear amino acid sequence of μ2 (22), and the structural model recently published by Wang et al. (49), residue 612 is not close to the NTP-binding motifs (Fig. 10). Moreover, residue 612 is not mapped to any known functional domain. It is possible that the altered residue (or its nearby region) affects nucleotides binding in several ways. First, the amino acid replacement may affect nucleotide-binding kinetics of μ2. For example, it has been found that purified T1L μ2 would hydrolyze ATP most effectively around pH 6.5 to 7.0 and at 35°C (we used similar experimental conditions to perform the *in vitro* NTP hydrolysis assay in Fig. 3B) (20), but these may not be the optimal conditions for the altered T3v10^{M1} μ2. Nevertheless, the T3v10^{M1} μ2 is most effective in hydrolyzing ATP and GTP (Fig. 3B), and this agrees with previous findings (20). Second, our data may suggest that T3v10^{M1} μ2 has a different affinity for NTP binding from T3wt μ2. For example, high concentration of NTPs may be needed for the mutant μ2 to achieve the same degree of substrate binding. This explanation seems to be supported by our data, which show that NTP hydrolysis of T3v10^{M1} μ2 was greatly impacted at 100-min and later time points, as the pool of available NTP was depleted (Fig. 3B). An alternative explanation is that the altered μ2 is more susceptible to product inhibition (58), and the released phosphate from NTP may bind μ2 and inhibit its enzymatic activities. In conclusion, our findings shed light on the relationship between the μ2 residue 612 and NTPase activities.

Previous studies performed an *in vitro* transcription assay (the same approach we employed for Fig. 3C) using the viral core and demonstrated that μ2 plays a key role in RNA synthesis and genome transcription (59–61). We sought to gain insights into how the A612V amino acid replacement impairs transcriptional activities from the *Aquareovirus* VP5 structural model. Until now, no architectural model of the mammalian *Orthoreovirus* λ3-μ2 transcriptional complex has been published. However, the near-atomic resolution structure of *Aquareovirus* VP2 (MRV λ3 homolog) and its cofactor VP5 (homolog of MRV μ2) complex has been discovered by Wang and colleagues, as discussed above (49). Pairwise alignment of the T3v10^{M1} μ2 amino acid sequence with that of the *Aquareovirus* VP5 (UniProt accession number Q8JU68) revealed that the 612 residues of the two homologs closely match with each other and that the residue belongs to the C-terminal domain (residues 600 to 700) of μ2/VP5 (22, 49). The VP5 residue 612 and remaining C-terminal residues are believed to interact with dsRNA approaching the transcriptional complex, since this C-terminal domain abuts the entrance where the RNA template enters the channel of VP2(λ3) (Fig. 10) (49). Furthermore, Wang and colleagues argued that VP5 may couple NTP hydrolysis to drive conformational change of the C-terminal domain, which may affect interactions between RNA templates and VP2 in the process of genome transcription (49); our data are consistent with the prediction made by Wang and colleagues. In summary, taking into account the published structural model of μ2 homolog VP5 and predictions by Wang and colleagues, we speculate that transcriptional activities of T3v10^{M1} μ2 could be impaired in two ways. First, residue 612 in the C-terminal loop might directly impact NTPase hydrolysis, and in that way impact the energy available for the loop to participate in template feeding. The reverse hypothesis might also be possible, where the 612 residue and the C-terminal loop directly impact template feeding, and reduced

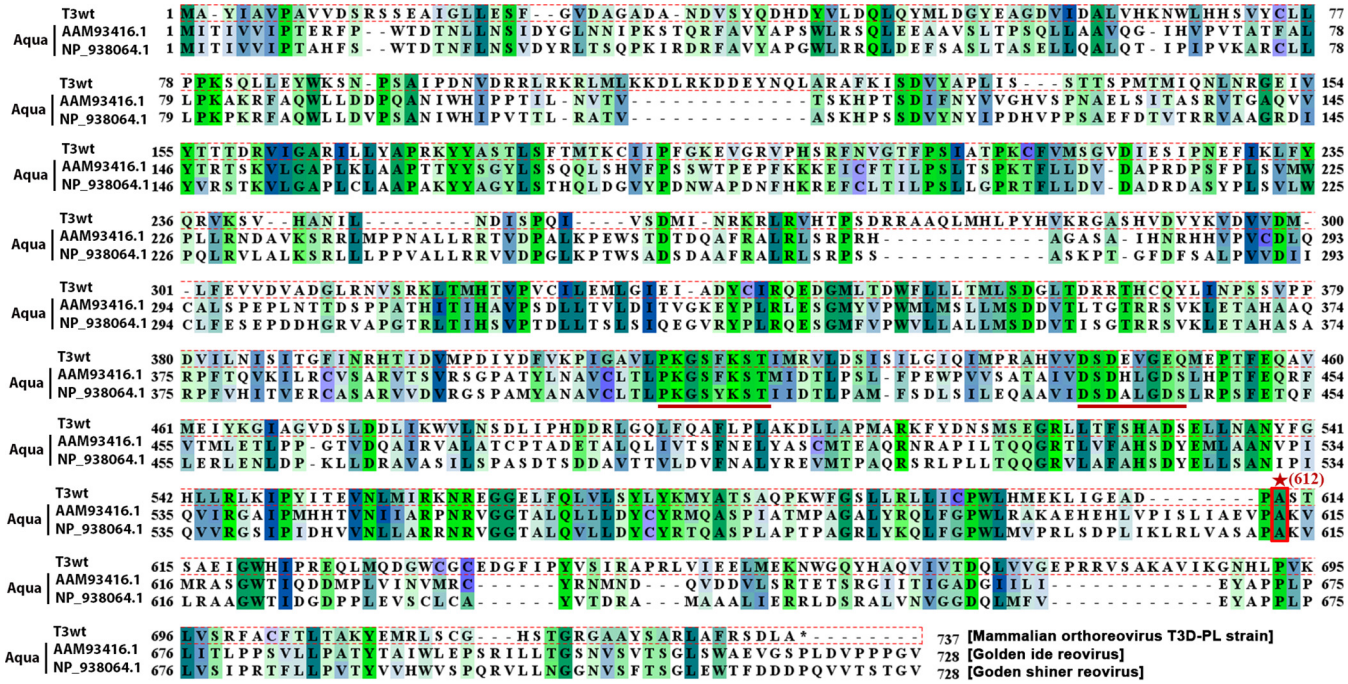

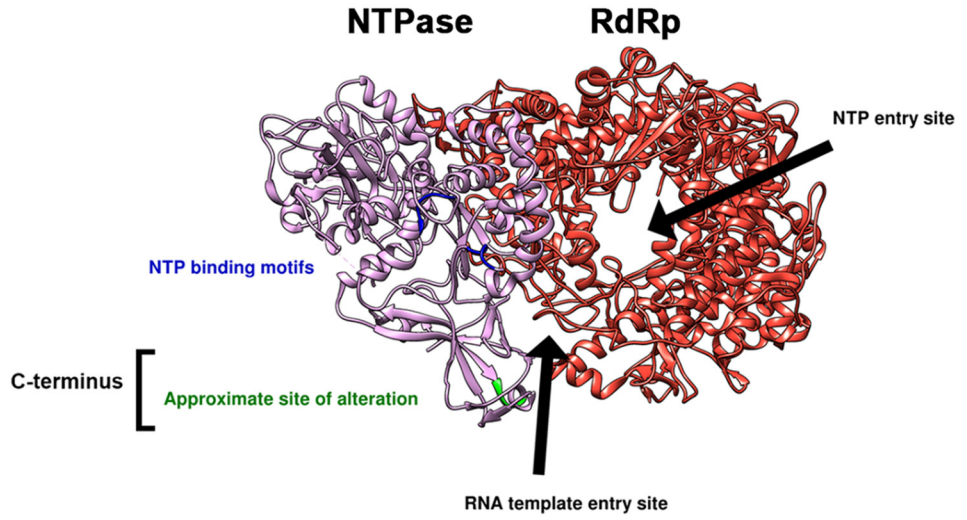

FIG 10 The T3v10^{M1} μ2 amino acid replacement is located in the uncharacterized C terminus. (Top) Sequences of T3wt μ2 (top sequence), were compared with those of two subspecies of *Aquareovirus* homolog VP5. The structure of VP5 has been recently published (bottom) from the middle sequence. The NTPase motifs are well conserved (underlined), but the T3wt residue 612 alanine (site with an *, replaced by valine in T3v10^{M1}) is located in the C terminus, which is not conserved among the three viruses. Note that all of the sequences were downshifted when the multiple alignment was performed. (Bottom) A 3D model of the transcription complex composed of the polymerase VP2(λ3) and its cofactor VP5(μ2). Due to the high homology between VP5 and μ2, a small region of the C terminus has been highlighted in green to represent the T3wt μ2 A612V alteration, which is located at the entrance of the RNA template entry site but not in close proximity to the NTP binding motifs. The C terminus of μ2 has not been characterized previously and is not associated with any known function.

flexibility and conformational activity of the loop in turn reduce processivity of NTPase hydrolysis. In either scenario, our data provide the first empirical support for a linked role of the μ2 C-terminal loop in NTPase and RNA synthesis.

Effects of the μ2 C-terminal domain on association with μNS. The A612V mutation enhanced the association of μ2 with μNS. Specifically, when assessing the association between μ2 and μNS in the absence of virus infection (i.e., the direct association between these proteins when expressed alone), there was a modest enhancement of ~2-fold; however, in the context of virus infection, where all processes are amplified, there became an ~8-fold enhanced association. The enhanced direct association of μ2

and μNS was confirmed using several diverse approaches such as coimmunoprecipitation and Far-Western blotting, but also during cotransfection or cotransfection/coinfection conditions. These experiments suggest that a modest enhanced direct interaction exists, which becomes further amplified during a virus infection.

It is not surprising to see μ2 complexed with μNS, since μ2 was already demonstrated to bridge μNS and tubulin and was proposed to facilitate virus assembly through interactions between μNS and other structural proteins (29, 30, 35, 62, 63). What is surprising is that the C-terminal loop of μ2 impacts interactions with μNS, since these previous studies implicated the opposite face of μ2 in μNS interactions. It will be interesting in the future to understand how the C-terminal μ2 loop affects μNS association.

The most straightforward explanation for enhanced progeny production by T3v10^{M1} relative to T3wt is that the A612V mutation in μ2 promotes recruitment of μNS, and that given that μ2-μNS are the foundation of factory formation and recruitment of virus components, the association directly enhances virus protein accumulation. Another possibility is that the morphology of the viral factories could change because of the A612V mutation in μ2. Previous studies found that a proline at position 208 of μ2 in the T1L serotype isolate forms filamentous factories, while a serine at the same position in the T3D serotype isolate forms globular factories (29, 31). The factory morphology differences have been attributed to differential association of viral factories with microtubules, which improves virus assembly and genome packaging, leading to increased virus replication (30). Interestingly, T3wt and T3v10^{M1} both have a proline in the 208 residue and exhibit similar factory morphologies (data not shown); however, we cannot exclude the possibility that the A612V mutation in T3v10^{M1} changes morphology in more subtle ways that promotes virus protein accumulation and the assembly of progeny virions. For both of these possible scenarios, increased core assembly would amplify viral RNA (Fig. 5A and B), protein (Fig. 5 C-E), and progeny production (Fig. 1G). It is interesting that the A612V mutation in μ2 did not just increase the rate of these virus replication steps but increased the overall RNA/protein maximum levels and virus burst size. In other words, wild-type reovirus RNA synthesis normally plateaus at ~12 hpi, and progeny production at ~20 hpi. This saturation point was exceeded by T3v10^{M1}, suggesting that μ2 activities are limiting during T3wt infection.

Potential implications for virus infection and oncolytic therapy applications. One of our favorite questions when we identify a mutation that enhances reovirus activity in cancer cells, is that of why the virus did not evolve this mutation to begin with. Since we could not find the A612V or similar polymorphisms among published μ2 sequences, we predict that it is not favorable "in nature." Based on our findings that this mutation comes with an "early" cost but a "late" benefit, the possibility is raised that viruses forgo late advantages for early advantages, perhaps because there is high pressure for limited numbers of incoming viruses to establish themselves. Interestingly, during infection of nontransformed NIH-3T3 cells, where reovirus only produces small foci of 2 or 3 infected cells reflecting poor infectious capacity, T3v10^{M1} seems even less infectious than T3wt (Fig. 1B and C). This very abstract concept, however, would need comprehensive testing in mouse models of enteric reovirus infection, where we would predict that T3wt would outperform T3v10^{M1}. When we artificially use reovirus for cancer therapy and administer 10^8 infectious particles, or during *in vitro* infection of cancer cells at moderate MOIs, the natural pressure for early stages of infection might be less influential.

The stoichiometric examination of our study also implores further considerations. Overall, the cost to virus transcription and establishment of infection in T3v10^{M1} was ~2- to 3-fold, while the benefit to *de novo* virus RNA and protein production was ~2- to 3-fold. In essence, these should cancel each other out to produce an equally infectious virus compared to T3wt. Clearly, however, T3v10^{M1} produces much larger plaques. Our finding that IRF3 is phosphorylated less during infection by T3v10^{M1} relative to that by T3wt reveals that the increased association of μ2 with μNS in T3v10^{M1} could promote additional aspects of reovirus infection that further augment plaque size.

As for applicability to cancer therapy, we originally isolated T3v10^{M1} in an attempt

to discover viruses that replicate better than T3wt in tumor cells and which therefore could be tested for cancer therapy. Our mechanistic studies on T3v10^{M1} both support and refute testing this specific virus *in vivo*. On the positive side, T3v10^{M1} presents a strategy to enhance late stages of reovirus replication in many cancer cells (Fig. 1B to G) while actually reducing infectivity in nontransformed cells (Fig. 1B and C). Moreover, it may be possible to combine the A612V mutation in μ2 with previously characterized mutations that enhance entry steps of reovirus replication, to further compound reovirus replication in tumor cells. However, since an oncolytic virus is likely to require high initial infectivity before immune clearance, our discovery that the A612V mutation in μ2 also drastically reduces establishment of infection (Fig. 3 and 4) suggests that T3v10^{M1} is not yet ready for *in vivo* oncolysis testing. Instead, we propose that a better fundamental understanding of μ2 could yield a strategy to uncouple the early versus late functions of this protein and enhance μ2-μNS association in the absence of reduced NTP hydrolysis and transcription. If this is possible, it will raise the question of why MRV did not evolve such an advantage in nature. Conversely, it is possible that the two functions of μ2 cannot be uncoupled and that MRV evolved a balance of the two functions at the expense of having a larger burst size.

MATERIALS AND METHODS

Cell lines and viruses. PanC, T47D, MCF7, TUBO, H1299, B16-F10, L929, and NIH3T3 cells were purchased from the American Type Culture Collection (ATCC). All cells were maintained and cultured according to ATCC recommendations. Reovirus serotype type 3 Dearing (T3wt) and variants were propagated from seed stocks to preserve genetic identity. All viruses were propagated in L929 cells. Infected cells were pelleted, lysed by freeze-thawing three times and Vertrel XF (Dymar Chemicals), and purified by ultracentrifugation on cesium chloride (CsCl) gradients, as previously described (64). Viruses T3wt and T3v10^{M1} were sequenced twice. First, in June 2015, only the S1, M1, and M2 genes; and second, in September 2017, the full virus genome. The A612V mutation was confirmed as the only missense mutation in T3v10^{M1} mutant.

Plaque size and titers. To compare plaque sizes of T3wt and variants, we performed plaque assays on the indicated cell lines as previously described (18). Plaques were visualized by immunocytochemical staining as previously described (18) or using a 1% (wt/vol) crystal violet solution. Plaque sizes were quantified with ImageQuant TL (Amersham Biosciences) or ImageJ. For titers of virus preparations or growth curves, plaque assays were done in L929 cells. Plaques were visualized after staining with a 1% (wt/vol) crystal violet solution and manually counted.

Generation and sequencing of reovirus variants. L929 cells were infected with T3wt at an MOI of 1 in the presence of 200 μM 5-fluorouracil. Morphological changes of cells were monitored by light microscope. When approximate 50% of cells showed cytolysis, cells were lysed by 3 rounds of freezing and thawing. To remove cell debris, cell lysate was centrifuged at 2,500 $\times$ *g* for 10 min. The supernatant was placed on top of a30% sucrose cushion and centrifuged at 100,000 $\times$ *g* for 1 h. The supernatant was discarded, and the virus pellet was resuspended with 200 μl phosphate-buffered saline (PBS). The titer and plaques of viral variants were determined and variants were isolated as previously described (18). To identify mutations for reovirus variants, all 10 genome segments reverse transcribed with SuperScript (Invitrogen) and PCR amplified with high-fidelity Vent polymerase (New England BioLabs), using 3′-end and 5′-end primers specific to each segment. PCR products from two preparations were then sequenced in both directions (MCLAB Sequencing Services), using forward and reverse primers that spanned the entire sequence in 300- to 400-nucleotide intervals for each direction. Sequences were assembled using Vector NTI software (Invitrogen). The 10 genome segments of variants were sequenced with at least 3 overlapping sequence reads per nucleotide.

Binding assays. To compare cell binding of reovirus, L929 cells at 100% confluence were prechilled at 4°C and exposed to reovirus for 1 h at 4°C with agitation every 5 min (all subsequent steps were performed at 4°C). Unbound virus was removed by three independent washes with ice-cold PBS. Cells were detached by treating with trypsin-EDTA (catalog no. 25200072; Gibco) and collected into 1.5-ml Eppendorf tube. Cells were pelleted by centrifugation at 1,000 $\times$ *g* for 5 min, followed by two washes with PBS. Cell pellets were either subjected to Western blot analysis or flash-frozen and stored at −80°C.

Agarose gel analysis of the whole reovirus. CsCl-purified reovirus was subjected to SDS-PAGE and quantified by Coomassie blue staining. Equivalent viral particles were diluted with 5% Ficoll and 0.05% bromophenol blue and subjected to electrophoresis on a 1.0% agarose gel in TEA buffer (40 mM Tris-HCl, 5 mM sodium acetate, and 1 mM EDTA [pH 7.3]) (42) at 10 mA for 16 h at room temperature. Reovirus-loaded agarose gel was rinsed with distilled water and stained with Coomassie blue overnight. Reovirus species were visualized by UV transillumination on the ImageQuant LAS4010 imager (GE Healthcare Life Sciences).

rNTP hydrolysis assays. Full virions of T3wt and T3v10^{M1} (previously subjected to SDS-PAGE and stained by Coomassie blue, standardized and qualified) were incubated with 16 μg/ml chymotrypsin (CHT) for 3 h in a water bath set to 37°C. Generation of was confirmed by SDS-PAGE and Coomassie blue staining. The rNTP hydrolysis reactions were performed using a 1.5-ml Eppendorf tube for the ease of manipulation and incubation. Reaction mixtures were transferred to 96-well plate (Cellstar) before

detection. For each reaction, 0.1 mM rATP/rCTP/rGTP/rUTP was used and incubated with viral core for various lengths of time (time points are described in Results) at pH of 7.0. The reaction mixtures were prepared using the phosphate assay kit (product no. ab65622; Abcam) according to manufacturer's instructions.

Western and far-Western blot analyses. Western blot analysis was performed as previously described (7, 17). For far-Western blot analysis, a few procedures were modified from Western blot analysis and are specified below. 10 percent native PAGE was prepared similarly to Western blot analysis, except that sodium dodecyl sulfate (SDS) was completely omitted. Running buffer (1×) and transfer buffer (1×) were prepared by diluting 10× Tris/glycine buffer (catalog no. 1610734; Bio-Rad) with double-distilled water. For transfer buffer, methanol was omitted, and 0.5% SDS (wt/vol) was added to the buffer. Transfer buffer was stored at 4°C and pH was adjusted to pH 7.5 just before use. PVDF membranes were used for protein transfer. Following blocking with 3% bovine serum albumin (BSA), PDVF member was incubated with 10 ml PBS containing purified μNS or cell lysate with transfected μNS or μ2. PVDF membrane was washed briefly with distilled water and incubated with 0.5% paraformaldehyde (PFA) for 30 min at room temperature. Sequential steps were performed as Western blot analysis. Specific rabbit polyclonal antireovirus antibodies were to probe for different reovirus proteins as previously described (7).

Plasmid constructions. To generate plasmid-based vectors expressing reovirus expressing M1 (T3wt or T3v10^{M1} with a 5′ or 3′ FLAG tag) and M3 genes. L929 cells in 6-well plate (CELLSTAR) were infected with T3wt or T3v10^{M1} at MOI of 10 or T3v10^{M1} at MOI of 30. Infection was stopped when 50% cells displayed cytopathogenic effect such as rounding, swelling, and clumping. Cells were washed with PBS twice and incubated with 1 ml of TRIzol (catalog no. 15596026; Invitrogen). Cell lysate was mixed thoroughly with TRIzol and transferred to a 1.5-ml Eppendorf tube. Chloroform (200 μl) was added to the mixture and mixed thoroughly, followed by 10 min of incubation at room temperature. The mixture was then centrifuged for 15 min at 12,000 × *g* at 4°C, and the top aqueous phase containing viral RNA was transferred to a new 1.5-ml Eppendorf tube. To pellet viral RNA, 0.5 ml 100% isopropanol was added to the tube, mixed thoroughly, and allowed to sit at room temperature for 10 min. The tube was centrifuged for 10 min at 12,000 × *g* at 4°C, and supernatant was discarded. The pellet was washed with 1 ml 75% ethanol and vortexed briefly, followed by centrifugation at 8,000 × *g* for 10 min at 4°C. Supernatant was discarded, and the pellet was air-dried for 5 min. The pellet was resuspended using 30 μl of UltraPure DNase/RNase-Free Distilled Water (catalog no. 10977015; Invitrogen). The M1 or M3 reovirus genes were cloned in pcDNA3.0. To generate the plasmid expressing the M3 gene, a viral M3 transcript was reverse transcribed to cDNA using a Moloney murine leukemia virus (M-MLV) (catalog no. 28025013; Invitrogen) according to the manufacturer's instructions, with a forward primer containing a KpnI site (5′-AAAGGTACCCCACCATGGCTTCATTCAAGGGATT-3′) and a reverse primer with an XhoI site (5′-GGGCTCGAGTTACAACTCATCAGTTGGAAC-3′). The final PCR product and pcDNA3.0 vector were digested with KpnI and XhoI, gel purified, and ligated to obtain the final plasmid. To generate plasmids expressing the T3wt or T3v10^{M1} M1 gene with a 5′ or 3′ FLAG tag, M1 mRNA was reverse transcribed to generate M1 cDNA using the method described above with a reverse primer gene containing the XbaI site (5′-GGGTCTAGATCACGCCAAGTCAGATCG-3′). M1 cDNA was joined a Flag tag on either the 5′ or 3′ end using the iProof high-fidelity PCR kit (catalog no. 1725331; Bio-Rad). The 5′ Flag tag was created using a forward primer with an HindIII site (5′-AAAAAGCTTCCACCATGGATTACAAGGATGACGACGATAAGGATTACAAGGATGACGACGATAAGGGTGGC-GGCATGGCTTACATCGCAGTTC-3′) and a reverse primer with reverse primer gene containing the XbaI site (5′-GGGTCTAGATCACGCCAAGTCAGATCG-3′). The 3′ Flag tag was generated using a forward primer with an HindIII site (5′-AAAAAGCTTCCACCATG GCTTACATCGCAGTTCC-3′) and a reverse primer with an XbaI site (5′-GGGTCTAGATCACTTATCGTCGTCATCCTTGTAATCCTTATCGTCGTCATCCTTGTAATCGCCGCCACCCGCCA AGTCAGATCGGAAAG-3′). Each PCR product and a pcDNA3.0 vector were digested with HindIII and XbaI, gel purified, and ligated to obtain the final plasmid. All plasmids were Sanger sequenced to verify the presence of desired inserts.

Transfections and immunoprecipitations. For transfections, H1299 cells in 6-well plate at 80 to 90% confluence were used for Flag-tagged μ2 or μNS transfection. One microgram of plasmid was used per sample. Transfection was performed using Lipofectamine 3000 transfection reagent (catalog no. L3000015; Invitrogen) according to the manufacturer's instructions. Cells were harvested and detached by Cellstripper (product no. 25-056-CI; Corning) at 24 h posttransfection according to the manufacturer's instructions. Cells were pelleted by centrifugation at 2,000 × *g* for 5 min. The cell pellet was lysed and resuspended in 200 μl filtered Co-IP lysis buffer (50 mM Tris [pH 7.4], 150 mM NaCl, and 0.5% NP-40 with protease inhibitor cocktail; Sigma). For immunoprecipitations, 25 μl of protein G magnetic beads (catalog no. LSKMAGG10; Millipore) was used per sample. The beads were washed twice with Co-IP lysis buffer and incubated with 5 μl of anti-tubulin (product code 12G10; DSHB), anti-μNS, anti-μ2, or anti-Flag (product code F1804; Sigma) for 2 h with agitation at room temperature. Excess antibody was washed three times with Co-IP lysis buffer. An equivalent volume of bead-antibody mixture was added to cell lysate and incubated for 2 h with agitation at room temperature or overnight at 4°C. Beads were pelleted by centrifugation at 2,000 × *g* for 5 min and subjected to Western blot analysis.

Flow cytometric and immunocytochemical staining of productively infected cells. To quantify the percentage of cells productively infected by reovirus, L929 cells were trypsinized at 12 and 15 h postinfection (hpi), washed once with PBS, and fixed with 4% PFA for 30 min on ice. Cells were washed once with PBS and then incubated in PBS containing 0.1% Triton X-100 and 3% bovine serum albumin (PBST-3% BSA) with a polyclonal antireovirus antibody (1:5,000) overnight at 4°C. Cells were washed once to remove excess antibodies and incubated with secondary anti-rabbit Cy2- or Cy5-conjugated antibodies (at 1:500 in PBST-3% BSA) with gentle mixing every 10 min for 1 h at room temperature. Cells

were washed once with PBS and resuspended in PBS with 2% fetal bovine serum (catalog no. 12103C; Sigma) and 1% ethylenediaminetetraacetic acid (catalog no. E6758; Sigma). Cell fluorescence was quantified with a FACScan flow cytometer (Becton, Dickinson) and analyzed by FCS Express 6 (De Novo Software). For the visualization of immunocytochemical staining of reovirus antigen-positive L929 cells, infection was performed by exposing cells to equivalent viral particles of T3wt or T3v10^{M1} (quantified by Western blotting). At 18 hpi, cells were washed once with PBS and fixed with 4% PFA for 30 min on ice. Cells were washed once with PBS and then incubated in PBS containing 0.1% Triton X-100 and 3% bovine serum albumin (PBST-3% BSA) with polyclonal antireovirus antibodies (1:5,000) overnight at 4°C. Cells were washed once to remove excess antibodies and incubated with mouse anti-rabbit alkaline phosphatase-conjugated secondary antibodies (at 1:500 in PBST-3% BSA) with gentle mixing every 10 min for 1 h at room temperature. Then cells were incubated with nitroblue tetrazolium–5-bromo-4-chloro-3-indolyl-phosphate (NBT/BCIP) in 10 mM Tris-HCl (pH 9.5) until reovirus antigen-positive purple staining was visible. The staining was stopped by the addition of TE buffer (10 mM Tris-HCl and 1 mM EDTA at pH 8.0).

***In vitro* reovirus core transcription assay and in-cell transcription assay.** Viral cores were obtained by the procedures described above and resuspended in a mixture containing 2 mM each ATP, CTP, GTP, and UTP, 100 mM Tris-HCl (pH 8.0), 10 mM $MgCl_2$, 100 μg/ml pyruvate kinase, 3.3 mM phosphoenolpyruvate, and 600 U/ml RNase inhibitor. For negative controls, ATP was omitted. The reaction mixtures were incubated at 40°C for the indicated durations. At the end of incubation, 400 μl TRIzol LS reagent (catalog no. 10296010; Invitrogen) containing 15 ng/ml green fluorescent protein (GFP) RNA generated using T7 RiboMAZ *in vitro* transcription reactions (Promega) (according to the manufacturer's instructions) was added to each sample for normalization. RNA was isolated and purified by the procedures described above. Reovirus and GFP RNA levels were quantified by iScript one-step RT-PCR kit with SYBR green (catalog no. 1708892; Bio-Rad). For the in-cell transcription assay, L929 cells were exposed to equal amounts of cell-bound T3wt or T3v10^{M1} as described above, and viral RNAs were collected by the procedures described above. Viral RNAs were purified using a GenElute total RNA purification kit (catalog no. RNB100-100RXN; Sigma) according to manufacturer's instructions and reovirus RNA levels were qualified as described above. For cycloheximide treatment, L929 cells were preexposed to 50 μg/ml of cycloheximide (catalog no. 66-81-9; Sigma) 30 min before exposure to reovirus. Treated medium was replaced every 6 h to ensure treatment efficiency.

Statistical analysis. Analyses were performed using GraphPad Prism version 8.3. Details of each analysis can be found in the figure legends. For nonlinear regression, significance of data was tested against null hypothesis, one curve for all data sets, with the alternative hypothesis being that the two data sets have different curves. In our cases, two straight lines are generated using the means of fold differences of RNA synthesis from all time points in the same experiment, one for T3wt and one for T3v10^{M1}. The slopes of the two lines were compared to determine whether they were significantly different.

ACKNOWLEDGMENTS

This work was funded by a Canadian Institutes of Health Research (CIHR) Cancer Research Society (CRS) project grant to M.S., a project grant from the Li Ka Shing Institute of Virology (LKSIoV) to M.S., a project grant from the Canadian Cancer Society Research Institute (CCSRI), a salary award to M.S. from the Canada Research Chairs (CRC), and infrastructure support from the Canada Foundation for Innovation (CFI). G.T., N.N., and M.K. received stipend funding from the University of Alberta Undergraduate Research Initiative (URI). F.C. received a stipend from the Faculty of Medicine and Dentistry (FoMD) Dean's Doctoral Award, an LKSIoV Doctoral Award, a La Vie en Rose Scholarship for Breast Cancer Research award through the Cancer Research Institute of Northern Alberta (CRINA), and the John and Rose McAllister Graduate Scholarship. W.K.W.Y. received stipend funding from the University of Alberta Faculty of Medicine and Dentistry.

Flow cytometry was performed at the University of Alberta Faculty of Medicine and Dentistry Flow Cytometry Facility, which receives financial support from the Faculty of Medicine and Dentistry and Canadian Foundation for Innovation (CFI) awards to contributing investigators. Bart Hazes provided assistance in creating the 3D model of μ2 using the *Aquareovirus* homolog VP5. Egor Tchesnokov and Brendan Todd advised on interpreting the data of the rNTP hydrolysis assay.

We declare no potential conflicts of interest.

REFERENCES

1. Sabin AB. 1959. Reoviruses: a new group of respiratory and enteric viruses formerly classified as ECHO type 10 is described. Science 130:1387–1389. https://doi.org/10.1126/science.130.3386.1387.
2. Silverstein SC, Christman JK, Acs G. 1976. The reovirus replicative cycle. Annu Rev Biochem 45:375–408. https://doi.org/10.1146/annurev.bi.45.070176.002111.
3. Anonymous. 2012. Reoviridae, p 541–637. *In* King AMQ, Adams MJ, Carstens EB, Lefkowitz EJ (ed), Virus taxonomy: ninth report of the International Committee on Taxonomy of Viruses. Elsevier, Amsterdam, Netherlands.
4. Pruijssers AJ, Dermody TS. 2016. Reovirus, p 337–360. *In* Reiss CS (ed), Neurotropic viral infections. Springer International, Cham, Switzerland.

5. Rosen L. 1962. Reoviruses in animals other than man. Ann N Y Acad Sci 101:461–465. https://doi.org/10.1111/j.1749-6632.1962.tb18886.x.
6. Marcato P, Shmulevitz M, Pan D, Stoltz D, Lee PW. 2007. Ras transformation mediates reovirus oncolysis by enhancing virus uncoating, particle infectivity, and apoptosis-dependent release. Mol Ther 15:1522–1530. https://doi.org/10.1038/sj.mt.6300179.
7. Shmulevitz M, Pan LZ, Garant K, Pan D, Lee PW. 2010. Oncogenic Ras promotes reovirus spread by suppressing IFN-beta production through negative regulation of RIG-I signaling. Cancer Res 70:4912–4921. https://doi.org/10.1158/0008-5472.CAN-09-4676.
8. Clements D, Helson E, Gujar SA, Lee PW. 2014. Reovirus in cancer therapy: an evidence-based review. Oncolytic Virother 3:69–82. https://doi.org/10.2147/OV.S51321.
9. Gong J, Sachdev E, Mita AC, Mita MM. 2016. Clinical development of reovirus for cancer therapy: an oncolytic virus with immune-mediated antitumor activity. World J Methodol 6:25–42. https://doi.org/10.5662/wjm.v6.i1.25.
10. Phillips MB, Stuart JD, Rodriguez Stewart RM, Berry JT, Mainou BA, Boehme KW. 2018. Current understanding of reovirus oncolysis mechanisms. Oncolytic Virother 7:53–63. https://doi.org/10.2147/OV.S143808.
11. Zhao X, Chester C, Rajasekaran N, He Z, Kohrt HE. 2016. Strategic combinations: the future of oncolytic virotherapy with reovirus. Mol Cancer Ther 15:767–773. https://doi.org/10.1158/1535-7163.MCT-15-0695.
12. Ferhat M. 2017. Oncolytic viruses: the next major breakthrough in cancer treatment. J Hum Virol Retrovirol 5:00141.10.15406/jhvrv.2017.05.00141. 10.15406/jhvrv.2017.05.00141.
13. Mohamed A, Clements DR, Gujar SA, Lee PW, Smiley JR, Shmulevitz M. 2019. Single amino acid differences between closely related reovirus T3D lab strains alter oncolytic potency *in vitro* and *in vivo*. J Virol 94:e01688-19. https://doi.org/10.1128/JVI.01688-19.
14. Mohamed A, Smiley JR, Shmulevitz M. 2020. Polymorphisms in the most oncolytic reovirus strain confer enhanced cell attachment, transcription, and single-step replication kinetics. J Virol 94:e01937-19. https://doi.org/10.1128/JVI.01937-19.
15. Mohamed A, Johnston RN, Shmulevitz M. 2015. Potential for improving potency and specificity of reovirus oncolysis with next-generation reovirus variants. Viruses 7:6251–6278. https://doi.org/10.3390/v7122936.
16. van den Wollenberg DJ, Dautzenberg IJ, van den Hengel SK, Cramer SJ, de Groot RJ, Hoeben RC. 2012. Isolation of reovirus T3D mutants capable of infecting human tumor cells independent of junction adhesion molecule-A. PLoS One 7:e48064. https://doi.org/10.1371/journal.pone.0048064.
17. Mohamed A, Teicher C, Haefliger S, Shmulevitz M. 2015. Reduction of virion-associated sigma1 fibers on oncolytic reovirus variants promotes adaptation toward tumorigenic cells. J Virol 89:4319–4334. https://doi.org/10.1128/JVI.03651-14.
18. Shmulevitz M, Gujar SA, Ahn DG, Mohamed A, Lee PW. 2012. Reovirus variants with mutations in genome segments S1 and L2 exhibit enhanced virion infectivity and superior oncolysis. J Virol 86:7403–7413. https://doi.org/10.1128/JVI.00304-12.
19. Dryden KA, Farsetta DL, Wang G, Keegan JM, Fields BN, Baker TS, Nibert ML. 1998. Internal/structures containing transcriptase-related proteins in top component particles of mammalian orthoreovirus. Virology 245:33–46. https://doi.org/10.1006/viro.1998.9146.
20. Kim J, Parker JS, Murray KE, Nibert ML. 2004. Nucleoside and RNA triphosphatase activities of orthoreovirus transcriptase cofactor $\mu 2$. J Biol Chem 279:4394–4403. https://doi.org/10.1074/jbc.M308637200.
21. Noble S, Nibert ML. 1997. Core protein $\mu 2$ is a second determinant of nucleoside triphosphatase activities by reovirus cores. J Virol 71:7728–7735. https://doi.org/10.1128/JVI.71.10.7728-7735.1997.
22. Yin P, Keirstead ND, Broering TJ, Arnold MM, Parker JS, Nibert ML, Coombs KM. 2004. Comparisons of the M1 genome segments and encoded $\mu 2$ proteins of different reovirus isolates. Virol J 1:6. https://doi.org/10.1186/1743-422X-1-6.
23. Nibert ML, Kim J. 2004. Conserved sequence motifs for nucleoside triphosphate binding unique to turreted reoviridae members and coltiviruses. J Virol 78:5528–5530. https://doi.org/10.1128/jvi.78.10.5528-5530.2004.
24. Brentano L, Noah DL, Brown EG, Sherry B. 1998. The reovirus protein $\mu 2$, encoded by the M1 gene, is an RNA-binding protein. J Virol 72:8354–8357. https://doi.org/10.1128/JVI.72.10.8354-8357.1998.
25. Yin P, Cheang M, Coombs KM. 1996. The M1 gene is associated with differences in the temperature optimum of the transcriptase activity in reovirus core particles. J Virol 70:1223–1227. https://doi.org/10.1128/JVI.70.2.1223-1227.1996.
26. Dales S. 1963. Association between the spindle apparatus and reovirus. Proc Natl Acad Sci U S A 50:268–275. https://doi.org/10.1073/pnas.50.2.268.
27. Mbisa JL, Becker MM, Zou S, Dermody TS, Brown EG. 2000. Reovirus $\mu 2$ protein determines strain-specific differences in the rate of viral inclusion formation in L929 cells. Virology 272:16–26. https://doi.org/10.1006/viro.2000.0362.
28. Novoa RR, Calderita G, Arranz R, Fontana J, Granzow H, Risco C. 2005. Virus factories: associations of cell organelles for viral replication and morphogenesis. Biol Cell 97:147–172. https://doi.org/10.1042/BC20040058.
29. Parker JS, Broering TJ, Kim J, Higgins DE, Nibert ML. 2002. Reovirus core protein $\mu 2$ determines the filamentous morphology of viral inclusion bodies by interacting with and stabilizing microtubules. J Virol 76:4483–4496. https://doi.org/10.1128/jvi.76.9.4483-4496.2002.
30. Shah PNM, Stanifer ML, Hohn K, Engel U, Haselmann U, Bartenschlager R, Krausslich HG, Krijnse-Locker J, Boulant S. 2017. Genome packaging of reovirus is mediated by the scaffolding property of the microtubule network. Cell Microbiol 19. https://doi.org/10.1111/cmi.12765.
31. Broering TJ, Parker JS, Joyce PL, Kim J, Nibert ML. 2002. Mammalian reovirus nonstructural protein microNS forms large inclusions and colocalizes with reovirus microtubule-associated protein $\mu 2$ in transfected cells. J Virol 76:8285–8297. https://doi.org/10.1128/jvi.76.16.8285-8297.2002.
32. Broering TJ, Arnold MM, Miller CL, Hurt JA, Joyce PL, Nibert ML. 2005. Carboxyl-proximal regions of reovirus nonstructural protein μNS necessary and sufficient for forming factory-like inclusions. J Virol 79:6194–6206. https://doi.org/10.1128/JVI.79.10.6194-6206.2005.
33. Broering TJ, Kim J, Miller CL, Piggott CD, Dinoso JB, Nibert ML, Parker JS. 2004. Reovirus nonstructural protein mu NS recruits viral core surface proteins and entering core particles to factory-like inclusions. J Virol 78:1882–1892. https://doi.org/10.1128/jvi.78.4.1882-1892.2004.
34. Broering TJ, McCutcheon AM, Centonze VE, Nibert ML. 2000. Reovirus nonstructural protein μNS binds to core particles but does not inhibit their transcription and capping activities. J Virol 74:5516–5524. https://doi.org/10.1128/jvi.74.12.5516-5524.2000.
35. Carvalho J, Arnold MM, Nibert ML. 2007. Silencing and complementation of reovirus core protein $\mu 2$: functional correlations with $\mu 2$-microtubule association and differences between virus- and plasmid-derived $\mu 2$. Virology 364:301–316. https://doi.org/10.1016/j.virol.2007.03.037.
36. Eichwald C, Kim J, Nibert ML. 2017. Dissection of mammalian orthoreovirus $\mu 2$ reveals a self-associative domain required for binding to microtubules but not to factory matrix protein μNS. PLoS One 12:e0184356. https://doi.org/10.1371/journal.pone.0184356.
37. Miller CL, Arnold MM, Broering TJ, Hastings CE, Nibert ML. 2010. Localization of mammalian orthoreovirus proteins to cytoplasmic factory-like structures via nonoverlapping regions of μNS. J Virol 84:867–882. https://doi.org/10.1128/JVI.01571-09.
38. Campbell JA, Schelling P, Wetzel JD, Johnson EM, Forrest JC, Wilson GA, Aurrand-Lions M, Imhof BA, Stehle T, Dermody TS. 2005. Junctional adhesion molecule a serves as a receptor for prototype and field-isolate strains of mammalian reovirus. J Virol 79:7967–7978. https://doi.org/10.1128/JVI.79.13.7967-7978.2005.
39. Boehme KW, Hammer K, Tollefson WC, Konopka-Anstadt JL, Kobayashi T, Dermody TS. 2013. Nonstructural protein σ1s mediates reovirus-induced cell cycle arrest and apoptosis. J Virol 87:12967–12979. https://doi.org/10.1128/JVI.02080-13.
40. Connolly JL, Rodgers SE, Clarke P, Ballard DW, Kerr LD, Tyler KL, Dermody TS. 2000. Reovirus-induced apoptosis requires activation of transcription factor NF-κB. J Virol 74:2981–2989. https://doi.org/10.1128/jvi.74.7.2981-2989.2000.
41. Poggioli GJ, Dermody TS, Tyler KL. 2001. Reovirus-induced ζ^{1s}-dependent G_2/M phase cell cycle arrest is associated with inhibition of $p34^{cdc2}$. J Virol 75:7429–7434. https://doi.org/10.1128/JVI.75.16.7429-7434.2001.
42. Larson SM, Antczak JB, Joklik WK. 1994. Reovirus exists in the form of 13 particle species that differ in their content of protein sigma 1. Virology 201:303–311. https://doi.org/10.1006/viro.1994.1295.
43. Ebert DH, Deussing J, Peters C, Dermody TS. 2002. Cathepsin L and cathepsin B mediate reovirus disassembly in murine fibroblast cells. J Biol Chem 277:24609–24617. https://doi.org/10.1074/jbc.M201107200.
44. Golden JW, Bahe JA, Lucas WT, Nibert ML, Schiff LA. 2004. Cathepsin S supports acid-independent infection by some reoviruses. J Biol Chem 279:8547–8557. https://doi.org/10.1074/jbc.M309758200.
45. Johnson EM, Doyle JD, Wetzel JD, McClung RP, Katunuma N, Chappell JD, Washington MK, Dermody TS. 2009. Genetic and pharmacologic alteration of cathepsin expression influences reovirus pathogenesis. J Virol 83:9630–9640. https://doi.org/10.1128/JVI.01095-09.

46. Chandran K, Farsetta DL, Nibert ML. 2002. Strategy for nonenveloped virus entry: a hydrophobic conformer of the reovirus membrane penetration protein micro 1 mediates membrane disruption. J Virol 76:9920–9933. https://doi.org/10.1128/jvi.76.19.9920-9933.2002.
47. Liemann S, Chandran K, Baker TS, Nibert ML, Harrison SC. 2002. Structure of the reovirus membrane-penetration protein, μ1, in a complex with its protector protein, σ^3. Cell 108:283–295. https://doi.org/10.1016/S0092-8674(02)00612-8.
48. Thete D, Danthi P. 2015. Conformational changes required for reovirus cell entry are sensitive to pH. Virology 483:291–301. https://doi.org/10.1016/j.virol.2015.04.025.
49. Wang X, Zhang F, Su R, Li X, Chen W, Chen Q, Yang T, Wang J, Liu H, Fang Q, Cheng L. 2018. Structure of RNA polymerase complex and genome within a dsRNA virus provides insights into the mechanisms of transcription and assembly. Proc Natl Acad Sci U S A 115:7344–7349. https://doi.org/10.1073/pnas.1803885115.
50. Zhang X, Walker SB, Chipman PR, Nibert ML, Baker TS. 2003. Reovirus polymerase lambda 3 localized by cryo-electron microscopy of virions at a resolution of 7.6 Å. Nat Struct Biol 10:1011–1018. https://doi.org/10.1038/nsb1009.
51. Madren JA, Sarkar P, Danthi P. 2012. Cell entry-associated conformational changes in reovirus particles are controlled by host protease activity. J Virol 86:3466–3473. https://doi.org/10.1128/JVI.06659-11.
52. Babiss LE, Luftig RB, Weatherbee JA, Weihing RR, Ray UR, Fields BN. 1979. Reovirus serotypes 1 and 3 differ in their *in vitro* association with microtubules. J Virol 30:863–874. https://doi.org/10.1128/JVI.30.3.863-874.1979.
53. Zamora PF, Hu L, Knowlton JJ, Lahr RM, Moreno RA, Berman AJ, Prasad BVV, Dermody TS. 2018. Reovirus nonstructural protein σ^{NS} acts as an RNA stability factor promoting viral genome replication. J Virol 92:e00563-18. https://doi.org/10.1128/JVI.00563-18.
54. Sherry B, Fields BN. 1989. The reovirus M1 gene, encoding a viral core protein, is associated with the myocarditic phenotype of a reovirus variant. J Virol 63:4850–4856. https://doi.org/10.1128/JVI.63.11.4850-4856.1989.
55. Irvin SC, Zurney J, Ooms LS, Chappell JD, Dermody TS, Sherry B. 2012. A single-amino-acid polymorphism in reovirus protein μ2 determines repression of interferon signaling and modulates myocarditis. J Virol 86:2302–2311. https://doi.org/10.1128/JVI.06236-11.
56. Stanifer ML, Kischnick C, Rippert A, Albrecht D, Boulant S. 2017. Reovirus inhibits interferon production by sequestering IRF3 into viral factories. Sci Rep 7:10873. https://doi.org/10.1038/s41598-017-11469-6.
57. Mohamed A, Konda P, Eaton HE, Gujar S, Smiley JR, Shmulevitz M. 2020. Closely related reovirus lab strains induce opposite expression of RIG-I/IFN-dependent versus -independent host genes, via mechanisms of slow replication versus polymorphisms in dsRNA binding σ^3 respectively. PLoS Pathog 16:e1008803. https://doi.org/10.1371/journal.ppat.1008803.
58. Frieden E, Walter C. 1963. Prevalence and significance of the product inhibition of enzymes. Nature 198:834–837. https://doi.org/10.1038/198834a0.
59. Demidenko AA, Nibert ML. 2009. Probing the transcription mechanisms of reovirus cores with molecules that alter RNA duplex stability. J Virol 83:5659–5670. https://doi.org/10.1128/JVI.02192-08.
60. Skehel JJ, Joklik WK. 1969. Studies on the *in vitro* transcription of reovirus RNA catalyzed by reovirus cores. Virology 39:822–831. https://doi.org/10.1016/0042-6822(69)90019-1.
61. Zarbl H, Hastings KEM, Millward S. 1980. Reovirus core particles synthesize capped oligonucleotides as a result of abortive transcription. Arch Biochem Biophys 202:348–360. https://doi.org/10.1016/0003-9861(80)90437-3.
62. Eichwald C, Ackermann M, Nibert ML. 2018. The dynamics of both filamentous and globular mammalian reovirus viral factories rely on the microtubule network. Virology 518:77–86. https://doi.org/10.1016/j.virol.2018.02.009.
63. Ooms LS, Jerome WG, Dermody TS, Chappell JD. 2012. Reovirus replication protein μ2 influences cell tropism by promoting particle assembly within viral inclusions. J Virol 86:10979–10987. https://doi.org/10.1128/JVI.01172-12.
64. Mendez II, Hermann LL, Hazelton PR, Coombs KM. 2000. A comparative analysis of Freon substitutes in the purification of reovirus and calicivirus. J Virol Methods 90:59–67. https://doi.org/10.1016/s0166-0934(00)00217-2.